Chapter 4

Studies on the Termination of Smectic A- Smectic A Phase Boundaries

4.1 Introduction

The smectic A phase formed of nonpolar molecules is, as a rule, of monolayer type where the layer spacing d is equal to the length of the molecule l. However in molecules having strong polar end groups, several types of smectic A phases with different periodicities have been identified. Studies on such materials has led to many interesting results like smectic A polymorphism and re-entrant phenomena. This chapter presents dielectric and X-ray experiments conducted on such materials exhibiting different types of smectic A phases and in addition a re-entrant nematic phase. We begin here with a brief introduction to smectic A polymorphism, followed by a summary of the phenomenological model due to Prost and coworkers which provides a satisfactory explanation of these phenomena. Experimental results near a critical point are presented. Finally results obtained in a novel phase diagram are also discussed.'

The chemical structure of a typical mesogen exhibiting monolayer smectic A phase (Sm A_1) is shown below. It consists of a central aromatic core which is

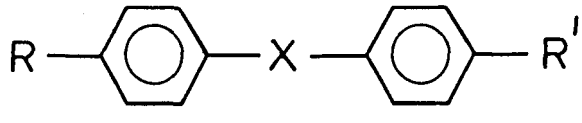

R & R' - flexible alkyl chain

X - linkage group

quite rigid with relatively flexible alkyl chain at one or both ends. Here X is the

linkage group. If the chain at one end is replaced by a strongly polar group like e.g., CN, NO_2, it is now established that other types of smectic A phases can exist. Madhusudhana and Chandrasekhar[1] predicted theoretically that in such polar systems, minimisation of the free energy demands antiparallel association of neighbouring molecules. One consequence of this antiparallel near-neighbour correlation is the formation of a smectic layer, whose thickness (d) is greater than the length of the molecule (l). Leadbetter et al. [2] showed the existence of such a bilayer structure wherein the aromatic cores overlap in the middle of a layer and the alkyl chains extend outwards (see figure 4.1). An interesting feature of such a pair is that it is more symmetric than the individual molecule. Synthesis of these materials with a strong polar end group opened a new field of study, namely, smectic A polymorphism.

Sigaud et al. [3] for the first time identified a transition between two different smectic A phases in binary mixtures of DB5CN and TBBA (see figure 4.2). Later, X-ray studies by Hardouin et al. [4] revealed that the higher temperature smectic A phase is a monolayer smectic A (Sm A_1) with layer spacing (d) being approximately equal to the length of the molecule and the lower one, bilayer smectic A (Sm A_2) with $d \simeq 2l$. In this notation the smectic A phase exhibited by compounds like 8CB, is a partially bilayer smectic A phase (Sm A_d), where $1 < d < 2l$ (see figure 4.1). These phases can be identified from the X-ray scattering pattern of monodonrain samples. Figure 4.3a & b shows a schematic representation of the molecular arrangement along with the characteristic X-ray diffraction pattern for the different types of smectic A phases. The notable features in the X-ray diffraction pattern are

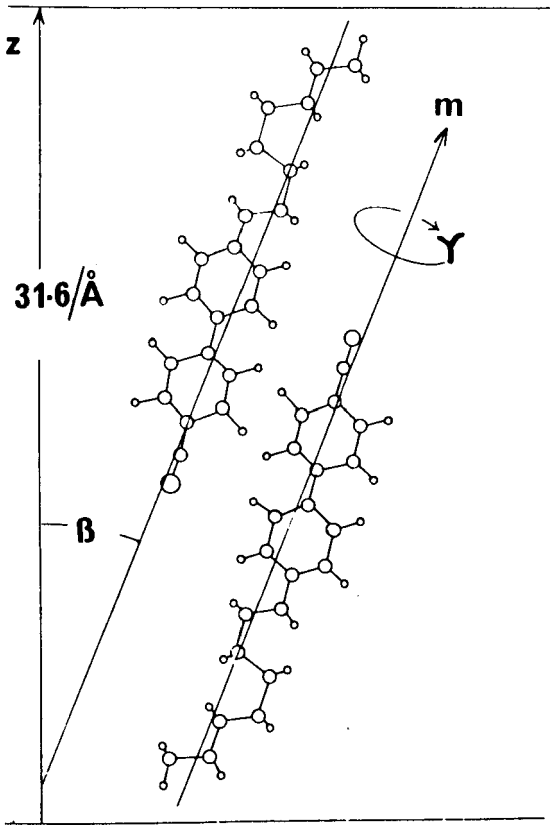

Figure 4.1: Schematic representation of the antiparallel arrangement in 8CB. (From Ref.2).

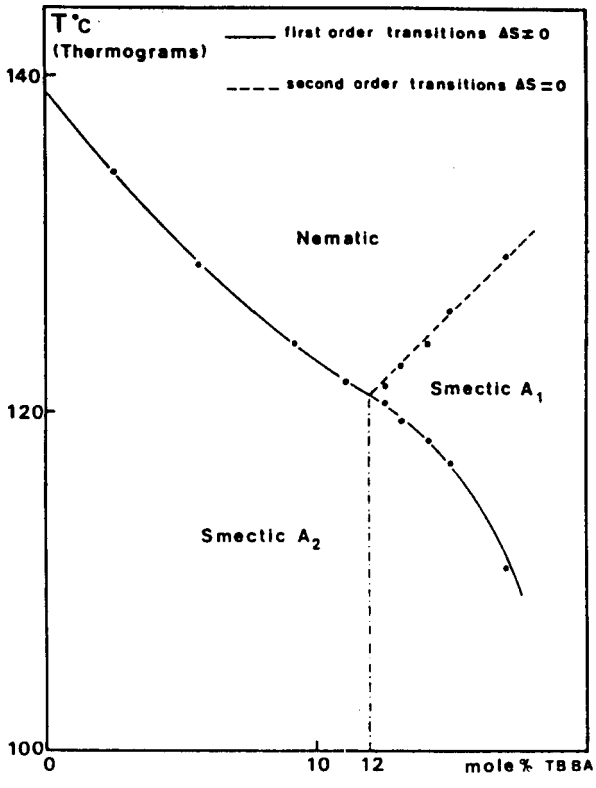

Figure 4.2: Part of DB5CN/TBBA phase diagram showing Sm A_1-Sm A_2 transition. (From Ref. 3).

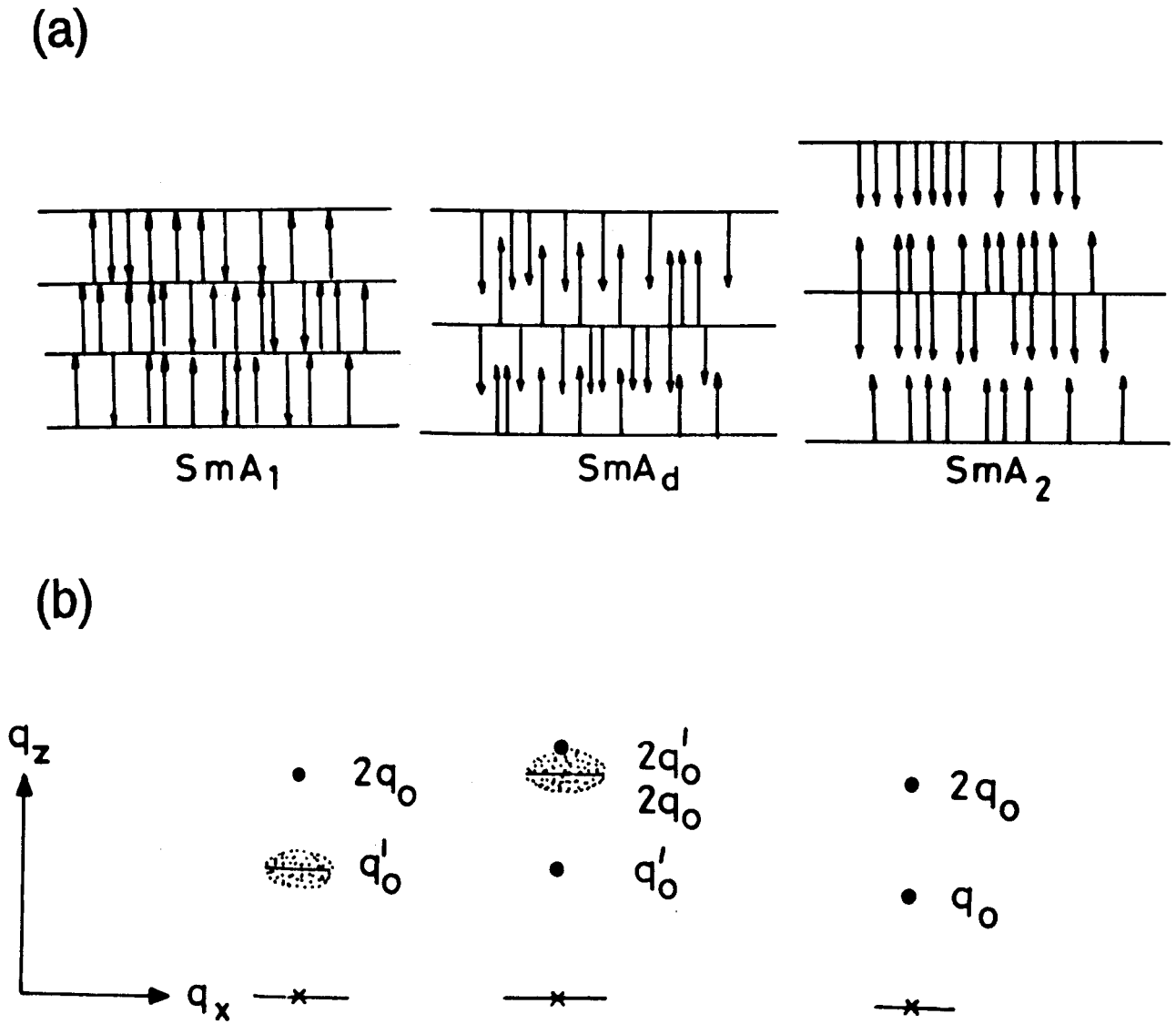

Figure 4.3: (a) Schematic representation of the molecular arrangement in Sm A_1, Sm A_d and Sm A_2 phases. (b) The cliaracteristic X-ray diffraction patterns for different types of smectic A phases. Here × denotes the direct bearn, q_z denotes the direction normal to the layer. Solid dot denotes condensed spot and the broad ring indicates a diffuse spot.

1. The monolayer Sm A_1 phase shows a condensed peak at a wavevector $2q_o(=2\pi/l)$. In addition, a diffuse scattering centered around $q_o'(=2\pi/l'$ where $l < 1' < 21$) is also seen.

2. The partially bilayer Sm A_d shows a condensed spot at q_o', a weak second harmonic at $2q_o'$ and a diffuse peak cehtred around $2q_o$.

3. The Sm A_2 phase shows condensed peaks at both q_o and $2q_o$, with q_o as fundamental and $2q_o$ as its second harmonic.

The occurrence of these polymorphic forms of smectic A phase is explained successfully by the phenomenological model introduced by Prost and coworkers.[5–7] They used this model within the frame work of the mean field theory to calculate the various theoretical phase diagrams[7] which involve transitions between these different types of smectic A phases. In the next section a brief discussion of this model is given with particular emphasis on some of the phase diagrams predicted.

4.1.1 Phenomenological model

In this model the free energy of smectic A is expressed in terms of two order parameters, *viz*, $\rho(r)$ describing the mass density order parameter, and $P_z(r)$, the dipolar order parameter associated with antiferroelectric ordering of the neighbouring molecules, along the z-axis. For Sm A_1, $P_z(r)=0$, whereas, for Sm A_2 phase both $\rho(r)$ and $P_z(r) \neq 0$. The competition between these two types of orders trying to condense at two incommensurate length scales leads to different

types of smectic A phases. Another offshoot of this feature is the re-entrant phenomena which we will not discuss here.

To describe the appearance of modulated order, order parameters $\rho(\mathrm{r})$ and $\mathrm{P}_z(\mathrm{r})$ are rewritten as,

$$P_z(r) = Re[\psi_1(r)] \qquad \rho(r) = Re[\psi_2(r)] \tag{4.1}$$

where $\psi_1(\mathrm{r})$ and $\psi_2(\mathrm{r})$ are complex fields:

$$\psi_1(\mathrm{r}) = \psi_1 e^{iq_p \cdot r} \qquad \psi_2(r) = \psi_2 e^{iq_\rho \cdot r} \tag{4.2}$$

In terms of these fields, the Landau-Ginzburg free energy in d-dimension in excess of the nematic free energy is

$$\begin{aligned} \Delta F \;=\; & \int d^d r \Big[\frac{1}{2} r_1 |\psi_1|^2 + \frac{1}{2} D_1 |(\Delta + k_1^2)\psi_1|^2 + \frac{1}{2} C_1 |\nabla_\perp \psi_1|^2 \\ & + \frac{1}{2} r_2 |\psi_2|^2 + \frac{1}{2} D_2 |(\Delta + k_2^2)\psi_2|^2 + \frac{1}{2} C_2 |\nabla_\perp \psi_2|^2 + u_1 |\psi_1|^4 \\ & + u_2 |\psi_2|^4 + 2u_{12} |\psi_1|^2 |\psi_2|^2 - w Re \psi_1^2 \psi_2^{*} \Big] \end{aligned} \tag{4.3}$$

where $\mathrm{r}_1 = a_1(T - T_{1c})$ and $\mathrm{r}_2 = a_2(T - T_{2c})$ measure the temperature from the non-interacting mean field transition temperatures T_{1c} and T_{2c} of the fields ψ_1 and ψ_2. $\nabla_\perp$ is a derivative in the plane perpendicular to the z-axis, parallel to $\vec{n}$. The elastic term $|(\Delta^2 + k_1^2)\psi_1|^2$ and $|(\Delta^2 + k_2^2)\psi_2|^2$ in equation **4.3** favour $q_p^2 = k_1^2$ and $q_\rho^2 = k_2^2$. The term Re $\psi_1^2 \psi_2^{*}$ favours lock-in at $q_\rho = 2q_p$.

This free energy leads to the following phases.

1. nematic phase with $|\psi_1| = |\psi_2| = 0$

2. Sm A_1 phase with $|\psi_1| = 0$, $|\psi_2| \neq 0$, $\mathrm{q}_\rho = k_2$ and

3. Sm A_2 phase with $|\psi_1| \neq 0$, $|\psi_2| \neq 0$ and $q_p = \frac{1}{2}q_\rho = q_o$

Note that an antiferroelectric smectic **A** phase with no long range mass density modulation ($|\psi_1| \neq 0$, $|\psi_2| = 0$) is never stable because a non-zero $|\psi_1|$ always generates a non-zero $|\psi_2|$ via the third order terms in ΔF_s.

For Sm A_1 phase the free energy density is obtained by minimizing

$$F_{Sm\ A_1} = \frac{1}{2}r_2|\psi_2|^2 + u_2|\psi_2|^4 \tag{4.4}$$

with respect to $|\psi_2|$.

The free energy density for the bilayer Sm A_2 phase is obtained by minimizing

$$\begin{aligned} F_{Sm\ A_2}\left(|\psi_1|, |\psi_2|, q_o\right) = {} & \frac{1}{2}\left[r_1 + D_1(q_o^2 - k_1^2)^2\right]|\psi_1|^2 + \frac{1}{2}\left[r_2 + D_2(4q_o^2 - k_2^2)^2\right]|\psi_2|^2 \\ & -w|\psi_1|^2|\psi_2| + u_1|\psi_1|^4 + u_2|\psi_2|^4 + 2u_{12}|\psi_1|^2|\psi_2|^2 \end{aligned} \tag{4.5}$$

with respect to $|\psi_1|$, $|\psi_2|$ and $\mathbf{q}_o$.

To proceed further they introduced rescaled variables

$$\psi_1 = 2\frac{w}{u_{12}}\sqrt{\frac{D_2}{D_1}}x\cos\theta \tag{4.6}$$

$$\psi_2 = \frac{1}{2}\frac{w}{u_{12}}x\sin\theta \tag{4.7}$$

so that

$$\bar{q_o}^2 = k_1^2\cos^2\theta + \frac{1}{4}k_2^2\sin^2\theta \tag{4.8}$$

where x measures the degree of order and θ the relative amplitudes of ψ_1 arid ψ_2. In terms of these variables the free energy density becomes,

$$\begin{aligned} f(x,\theta) = {} & x^2(y_1\cos^2\theta + y_2\sin^2\theta + z^2\cos^2\theta\sin^2\theta) - 2x^3\cos^2\theta\sin\theta \\ & + x^4(1 + \partial u_1\cos^4\theta + \partial u_2\sin^4\theta) \end{aligned} \tag{4.9}$$

where,

$$y_1 = 2\frac{u_{12}}{w^2}r_1, \quad y_2 = \frac{1}{8}\frac{D_1}{D_2}\frac{u_{12}}{w^2}r_2$$

$$z^2 = \frac{2D_1u_{12}}{w^2}\left(k_1^2 - \frac{1}{4}k_2^2\right)^2$$

$$\partial u_1 = 16\frac{u_1}{u_{12}}\frac{D_2}{D_1} - 1, \quad \partial u_2 = \frac{1}{16}\frac{u_2}{u_{12}}\frac{D_1}{D_2} - 1 \tag{4.10}$$

where y_1 and y_2 are the temperature variables, and z^2 is the incommensurability parameter measuring the degree of mismatch between k_1 and $k_2/2$. The usual stability requirements on fourth order terms require $\partial u_1, \partial u_2$ to be greater than -1. Numerical calculations performed by Barois et al.,[7] to minimize the free energy have led to a variety of phase diagrams. Only the relevant phase diagrams are discussed here.

4.1.2 Phase Diagrams

Case 1

For small incommensurability parameter z^2 and symmetric elastic and fourth order terms ($\partial u_1 = \partial u_2$) the phase diagram is shown in figure 4.4. The special features of this diagram are (1) Nematic-Sm A_1 boundary is second order throughout and terminates at a critical end point Q where N, Sm A_1, Sm A_2 phases meet. (2) There are two tricritical points, viz., R on Sm A_1-Sm A_2 and P on the N-Sm A_2 boundary.

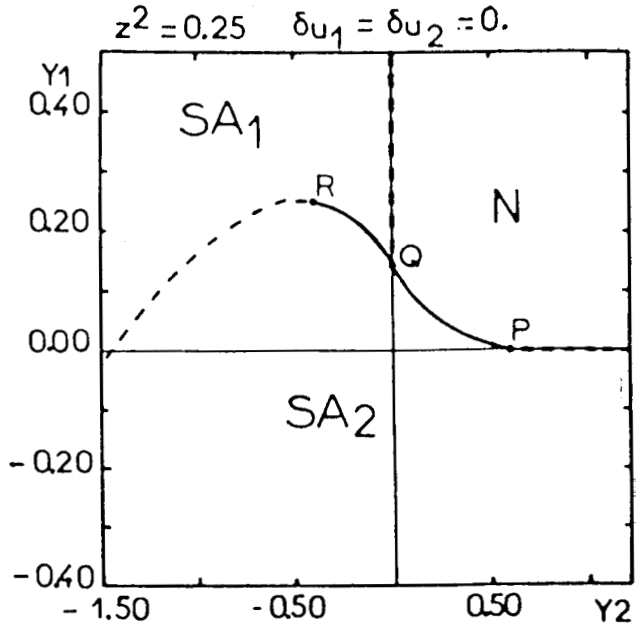

Figure 4.4: Phase diagram in the $y_1 - y_2$ plane lor small incommensurability parameter $z^2 = 0.25$, and the potentials $\partial u_1 = \partial u_2 = 0$. Solid (or dashed) line correspond to first (or second) order transition. Here Q is a critical end point, P and R are tricritical points. (From Ref. 7).

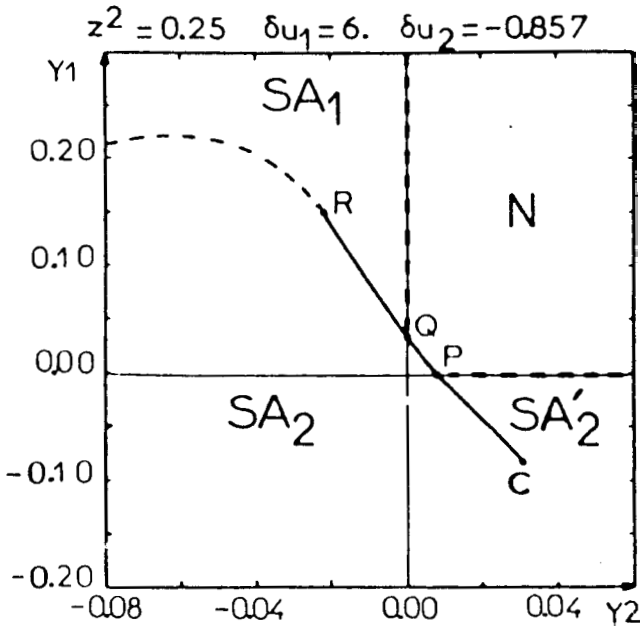

Figure 4.5: Phase diagram for $z^2 = 0.25$ with asymmetric potentials $\partial u_1 = 6, \partial u_2 = -0.857$. Solid (or dashed) line correspond to first (or second) order transition. Notice that the first order Sm A_2-Sm A_2' (or Srn A_d) phase boundary ends up at a *critical point* C followed by a continuous evolution region. (From Ref.7)

Case 2

If the elastic constants D_1 and D_2 are different and favour an easy compression of ψ_1 (i.e., ∂u_1 increases and ∂u_2 decreases), then, at small values of z^2, a new first order phase boundary separating two smectic A_2 phases appears (see figure 4.5). The two smectic A_2 phases are distinguished by different values of 8 and from equation 4.8 different values of q,. For small 8, q_o is of the order of k_1, and ψ_1 is much larger than ψ_2. Hence the Sm A_2' can be identified with the experimentally observed Sm A_d phase even though ψ_2 is strictly speaking non-zero.

For $0 < \theta < \pi/2$, tlie amplitudes of ψ_1 and ψ_2 are comparable leading to the Sm A_2 phase. The discontinuities in $\bar{q}_o^2$ and $\sin^2\theta$ across the new phase boundary are

$$\Delta\bar{q}_o^2 = \left(\frac{k_2^2}{4} - k_1^2\right)\Delta(\sin^2 8) \tag{4.11}$$

The new phase boundary is tangent to the first order N-Sm A_2 line at P and terminates at. a critical point C where $\Delta\bar{q}_o^2$ goes to zero. In the framework of mean field theory critical fluctuations in the vicinity of C are expected to be similar to those encountered at the liquid-gas critical point. The presence of the critical point C indicates, as expected, that there is no difference in symmetry between tlie Srn A_2 and Sm A', (or Sm A_d) phase with different relative amplitudes of ψ_1 and ψ_2.

Thus we see here that competition between ordering at two different length scales results in the formation of the three phases Sm A_1, Sm A_d and Sm A_2. These phases have the same macroscopic symmetry (i.e., one dimensional mass density wave along the optic axis or the layernormal) but differ from each other

only in the values of d. It is possible to go from Sm A_1 to Sm A_d or from Sm A_d to Sm A_2 phase merely by a contiriuous variation the layer spacing d. First order transitions in which there is discontinuous change in the wave vector q_o (i.e., Sm A_1-Sm A_d or Sm A_d-Sm A_2 transition) are always possible. A line of such first order transitions may terminate at a critical point[7,8] where the difference in wave vector between the two phases goes to zero. Such a critical point provides a continuous path coexisting between Sm A_1 (or Sm A_2) and Sm A_d phases. But the situation is different for Sm A_1-Sm A_2 transition. It can be either first order or second order. The latter is due to the exact doubling of the layer periodicity.

This chapter discusses two important results, namely,

1. Precise dielectric measurement near the Sm A_d-Sm A_2 critical point in a binary liquid crystalline system.

2. The existence of a continuous thermodynamic path between Sm A_1 and Sm A_2 phases.

4.2 The Sm A_d - Sm A_2 critical point

The first experimental observation of the Sm A_d-Sm A_2 critical point was in a binary system of 4-n-undecyloxyphenyl-4′-(4″-cyanobenzyloxy) benzoate (or 11OPCBOB) and 4-n-nonyloxybiphenyl-4'-cyano benzoate (or 9OBCB), employing high resolution X-ray techniques[g] Subsequently, high resolution calorimetric studies[10] were conducted on the same system which confirmed the conclusions arrived at from the X-ray studies. Results of these experiments performed by Shashidhar et a1[9] is shown in figure 4.6. It is observed that the strength of

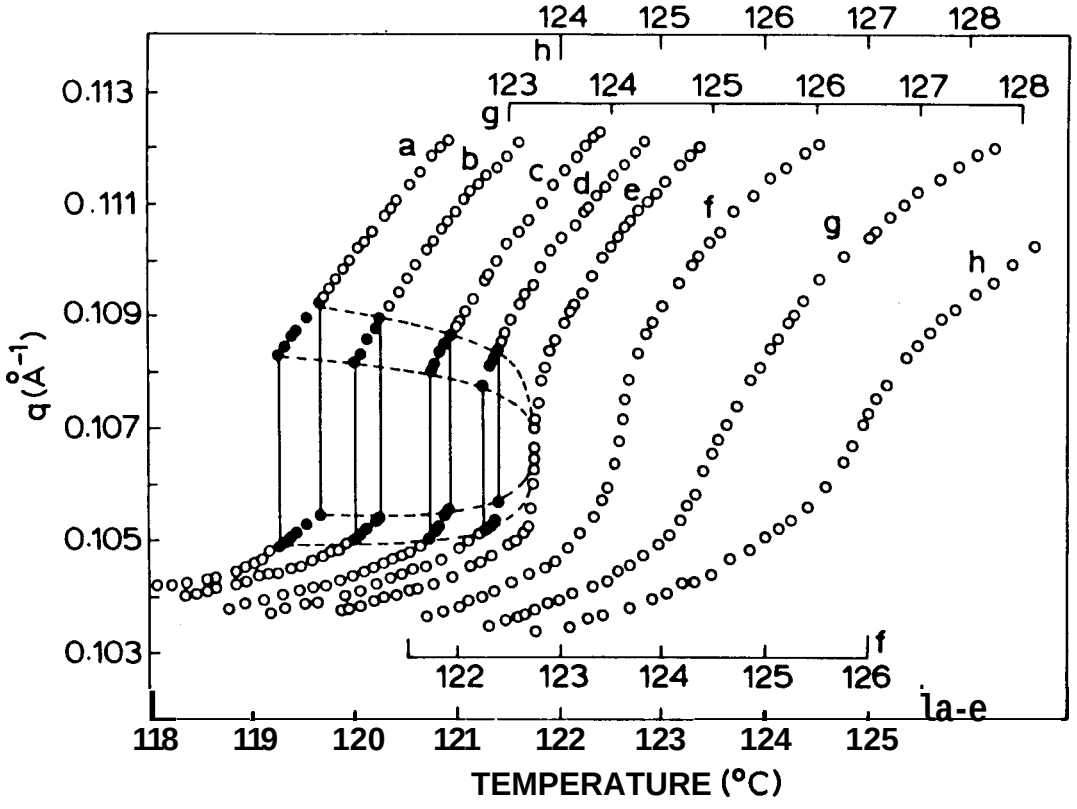

Figure 4.6: Plots of wave vector q_o, q_o' vs. temperature(T) for different mixtures of 11OPCBOB in 9OBCB. The mole-fraction(X) of 11OPCBOB in the mixture are a) 0.55, b) 0.571, c) 0.597, d) 0.619, e) 0.642, f) 0.715, g) 0.8 and h) 1.0. The corresponding temperature scales are identified. For X<0.642(plots a-d), first order Sm A_d-Sm A_2 transition is seen which manifests as a jump in the wavevector. The data in the two phase region are shown with filled circles, while the dashed line represent the width of two phase region. The critical point CP is identified by the vertical inflection point seen for X=0.642(plot e). (From Ref. 9).

the first order transition, characterised by a two-phase coexistence region and an accompanying jump in wave vector, decreases with increasing concentration, vanishes to zero at X=0.642, beyond which the wave vector varies continuously between tlic two pliascs.

Since the constituent molecules are polar and the extent of interdigitation of molecules in the neighbouring layers vary from one phase to another, one can expect the changes to be reflected in dielectric measurements also. In fact, earlier dielectric studies on materials having different smectic A phases have shown this to be true.[11–14] We present here precise dielectric measurements on the same binary system, viz., 11OPCBOB and 9OBCB, which again reveal the critical point in a striking fashion.

4.2.1 Experimental

The structural formulae and transition temperatures of 11OPCBOB and 9OBCB[15] are given in Table 4.1.

Dielectric setup

Dielectric experiments were conducted using a setup that was available in the laboratory.[12] A schematic diagram of the cell and the heater assembly is shown in the figure 4.7. The cell is rnade of two aluminium coated glass plates which serve as electrodes. The thickness of the cell is defined by a mylar spacer (thickness „ 25μ). The samples were filled in the isotropic phase by capillary action. The cell is held rigidly inside a copper frame with the help of a rectangular

11OPCBOB

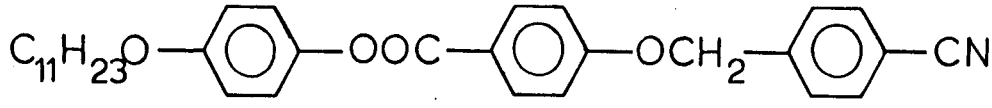

4-n-undecyloxyphenyl-4'-(4''-cyanobenyloxy) benzoate

Isotropic $\xrightarrow{}$ N $\xrightarrow[154.5]{}$ Sm A_d $\xrightarrow{}$ Sm A_2 $\xrightarrow[106]{}$ K
153.3

90BCB

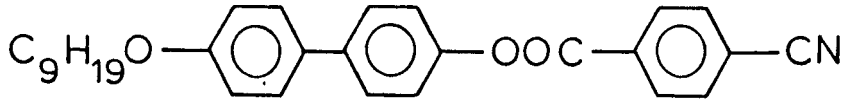

4-n-nonyloxybiphenyl-4'-cyanobenzoate

Isotropic $\xrightarrow{}$ N $\xrightarrow[207.8]{}$ Sm A_d $\xrightarrow[142.8]{}$ Sm $\tilde{C}$ $\xrightarrow[112.6]{}$ K
228.3

Table 4.1: Structural formulae and transition temperatures (in °C) of 11OPCBOB & 9OBCB.

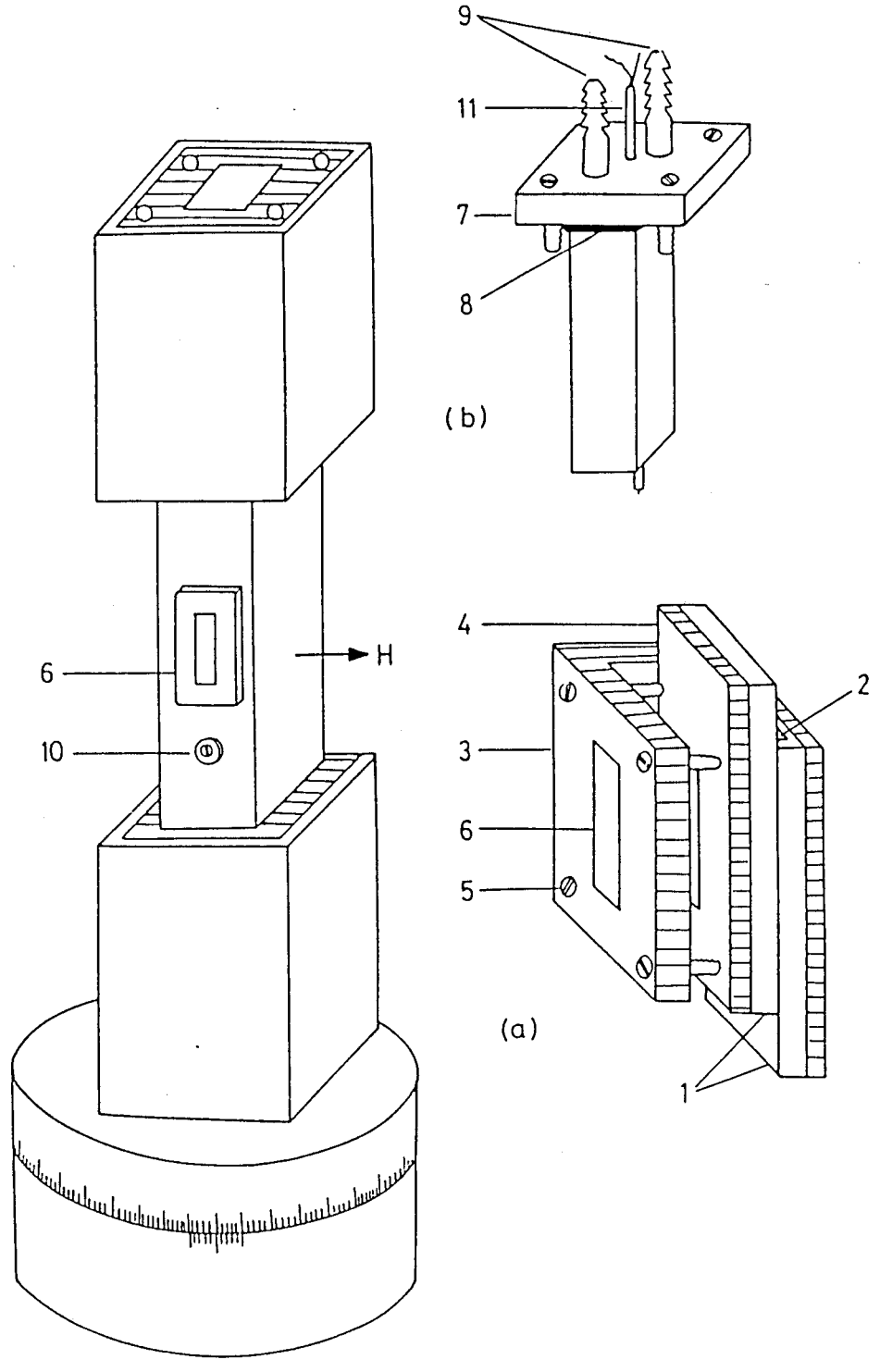

Figure 4.7: Schematic diagrarn of the cell arid heater assembly. 1. Electrodes, 2. Bevel, 3. Copper clamp, 4. Copper plate, 5. Brass screws, 6. Windows, 7. Copper cap, 8. Neoprene gasket, 9. Nozzles, 10. Brass nuts with pyrophilite brushes, 11. Chromel-constant an thermocouple. H represents the direction of magnetic field.

'G' clamp. Electrical contacts are made with the extended area of the glass plates. This cell assembly was positioned inside the central part of the heater. Nichrome tape wound on the top and bottom side of the heater assembly facilitated temperature control of the cell. The heater assembly was covered with hylum sheets for good thermal insulation. The assembly was mounted on a rotatable stage enabling positioning of the sample for measurements of both parallel and perpendicular components of the dielectric constants. The temperature of the sample was measured with the help of chromel-constantan thermocouple in conjunction with a low drift digital nanovoltmeter (Keithley, Model 181). The samples were aligned by cooling slowly (2-3° C/hour) from the nematic phase in the presence of a 2.4T magnetic field provided by an electromagnet (Bruker B-E 25). The capacitance of the cell is measured using a variable frequency Impedance Analyser[HP 4192A]. This instrurnent can be used to measure eleven impedance associated parameters such as capacitance C, conductance G, susceptance B, Dissipation or dielectric loss factor D, etc., with a basic accuracy of 0.1% throughout the range of measurement. The oscillating or measuring voltage is kept at 1 V rms. The principle of capacitance measurement is based on vector-voltage-current ratio measurement method. The capacitance measuring range is 0.1 pf to 100 mf arid that of the dielectric loss factor is 0.0001 to 19.999. Experiments were done in the four probe configuration which eliminates errors due to residual impedance of test leads. The dielectric constant of the sample is given by the ratio of capacitance of the sample to that of an empty cell.

The block diagram of the experimental setup used is shown in figure 4.8. Both the temperature measuring digital multimeter (Keithley 181) arid the

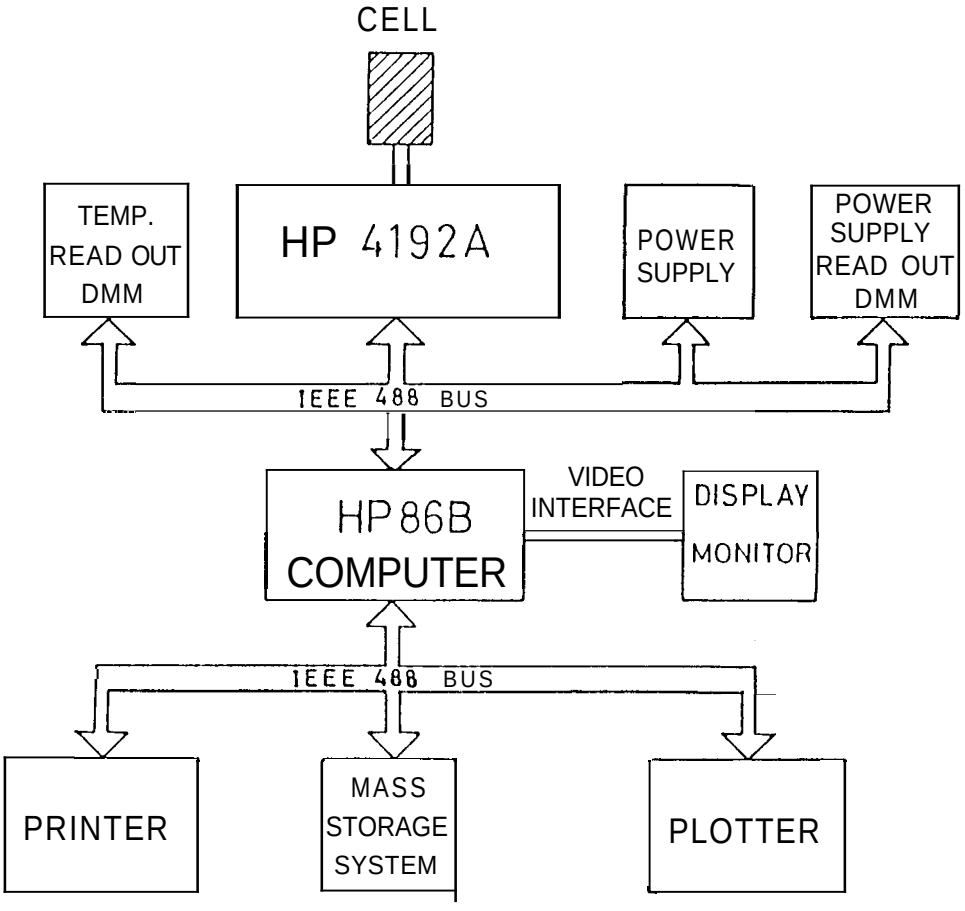

Figure 4.8: Block diagram of the experimental setup.

impedance analyser (HP4192A) were interfaced with a micro-computer (HP86B) through HPIB (IEEE 488) bus for data acquisition arid storage purpose. The static dielectric constants, $\epsilon_{\|}$ and $\epsilon_{\perp}$, parallel and perpendicular to the director respectively were measured at 10kHz, a frequency which is well below the relaxation frequency of any mode in the system, by varying the temperature of the sample at a uniform rate of 4-5°C/hour across the transition. Dispersion measurements were done by stabilising the sample temperature at a particular value and the frequency was swept from 1kHz to 13 MHz at a desired step value.

4.2.2 **Results and Discussion**

The temperature-concentration (T-X) phase diagram of 11OPCBOB-9OBCB system obtained by Shashidhar et al.,[9] is shown in the figure 4.9. Here X is the mol fraction of 11OPCBOB in in the mixture. From the phase diagram it is seen that for X<0.52 the ribbon phase Sm $\tilde{C}$ intervenes between Sm A_d and Srn A_2 phases. (Sm $\tilde{C}$ is an antiphase. In this phase the local order is tilted-Sm A_2 like but the direction of dipolar heads alternates periodically within a layer and this results in a rectangular symmetry). However, with increasing X, Sm $\tilde{C}$ is suppressed, leading to a direct Sm A_d-Sm A_2 transition. This first order Sm A_d-Sm A_2 phase boundary then terminates at a critical point followed by continuous evolution region.

Static dielectric constant measurements were done on 8 mixtures and the pure compound 11OPCBOB. Figures 4.10-4.18 show the thermal variation of $\epsilon_{\|}$ and $\epsilon_{\perp}$ in the Sm A_d and Sm A_2 phases for X=0.55, 0.59, 0.63, 0.65, 0.68,

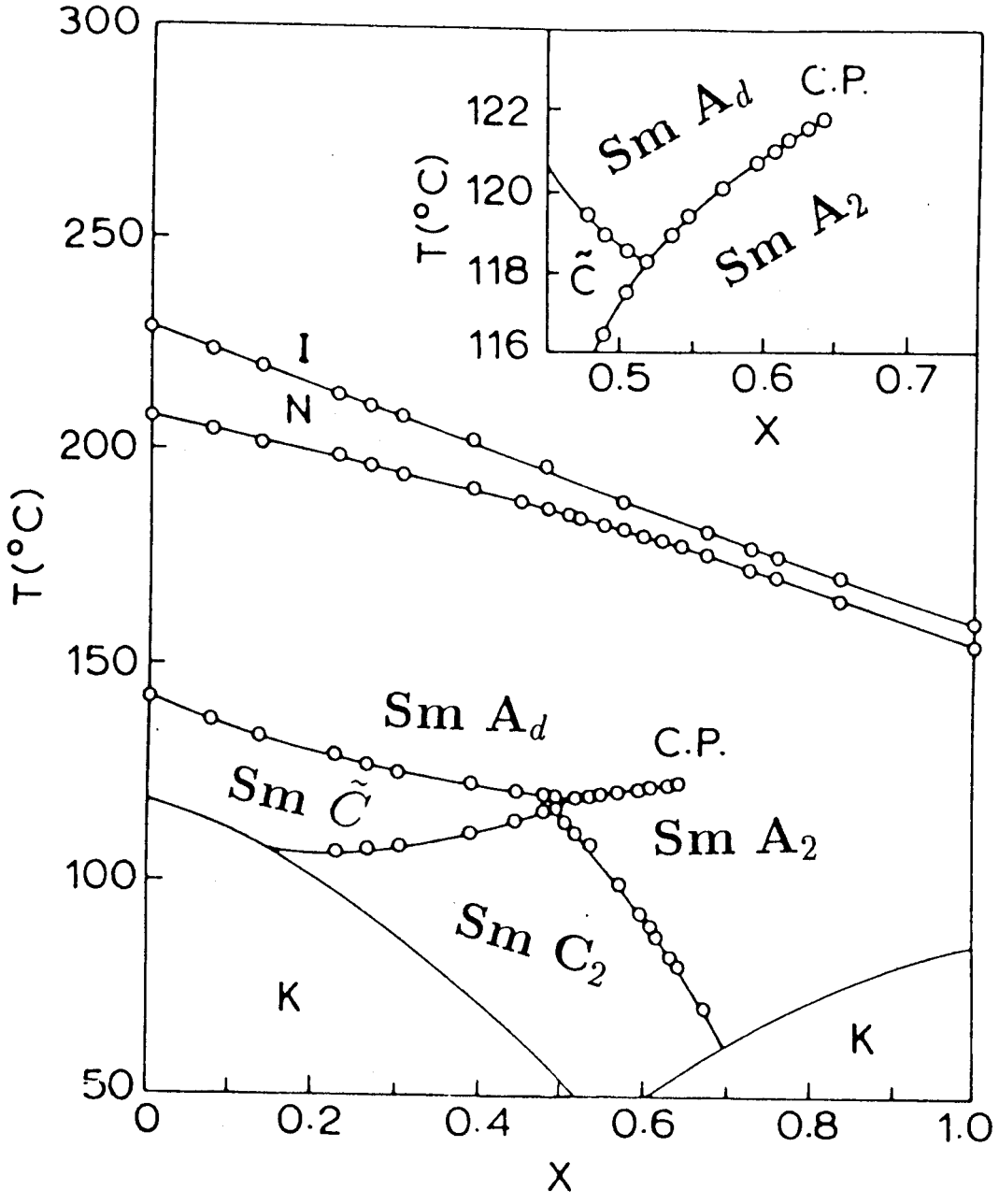

Figure 4.9: Temperature-concentration (T-X) phase diagram for the binary mixture of 11OPCBOB in 9OBCB. X is the mole fraction of 11OPCBOB in the mixture. First order Sm A_d-Sm A_2 transition terminates at the critical point (CP). Inset shows the phase diagram in the vicinity of CP on an enlarged scale. K → crystal, N → nematic, I → isotropic, Sm $\tilde{C}$ → antiphase Sm 6, Sm C_2 → bilayer Sm C_2 phase. (From Ref. 9).

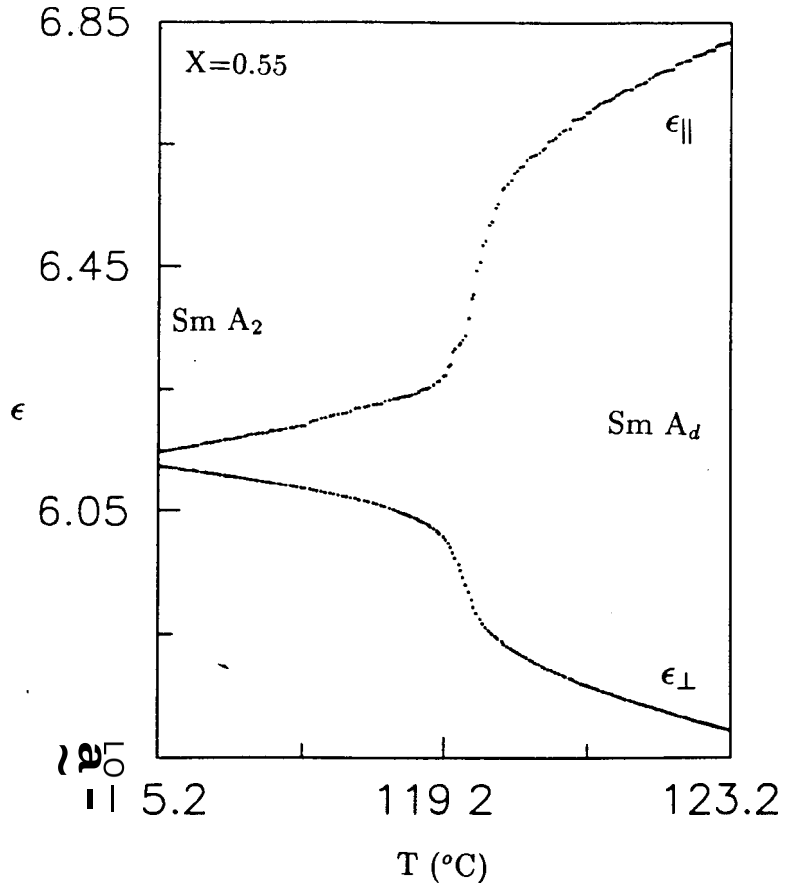

Figure 4.10: Temperature variation of $\epsilon_{\|}$ and $\epsilon_{\perp}$ for X=0.55.

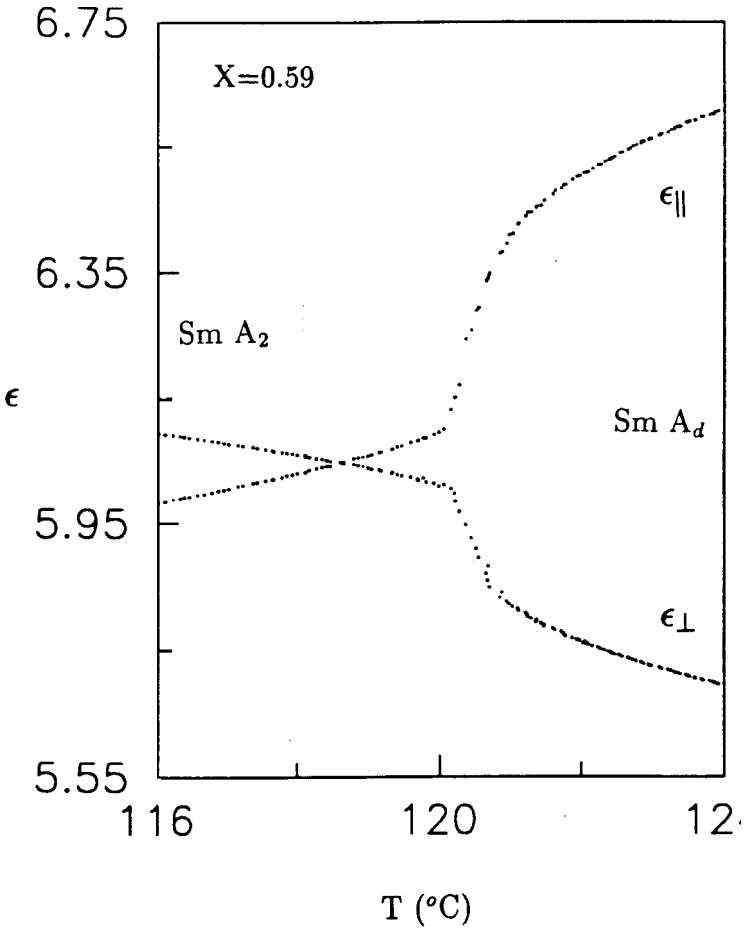

Figure 4.11: Thermal variation of $\epsilon_{\|}$ and $\epsilon_{\perp}$ for X=0.59

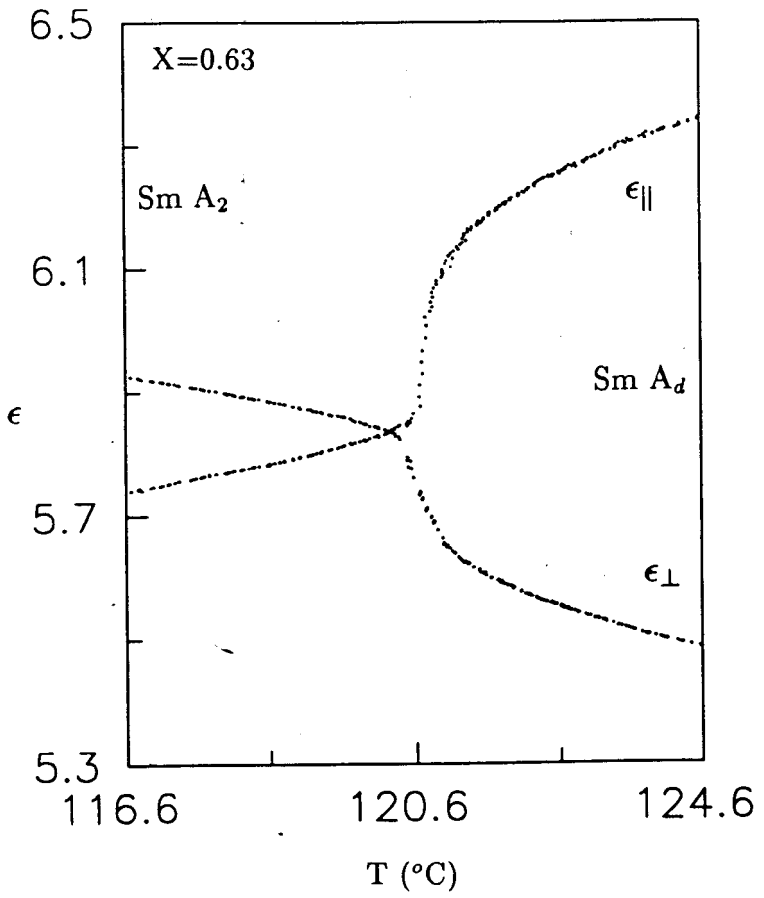

Figure 4.12: Thermal variation of $\epsilon_{\|}$ and $\epsilon_{\perp}$ for X=0.63.

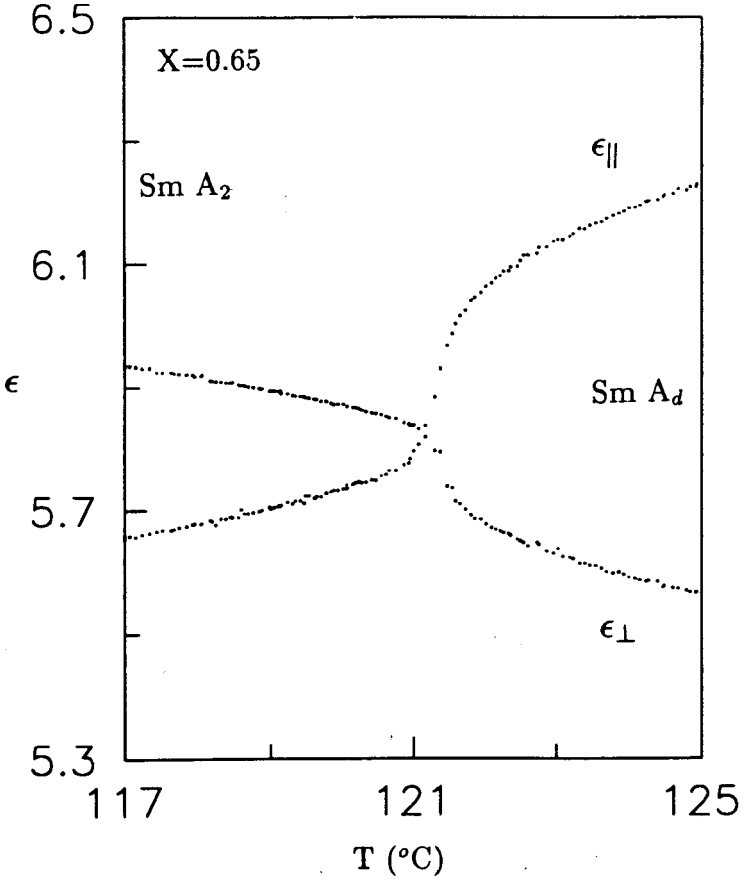

Figure 4.13:Temperature variation of $\epsilon_{\|}$ and $\epsilon_{\perp}$ for X=0.65.

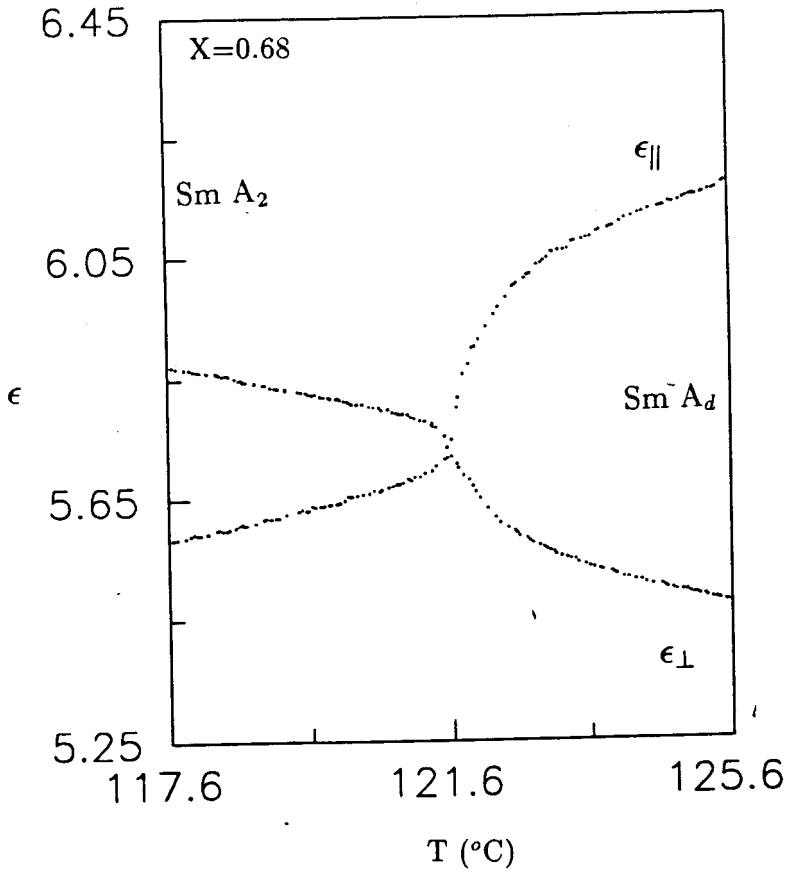

Figure 4.14: Temperature variation of $\epsilon_{\|}$ and $\epsilon_{\perp}$ for X=0.68.

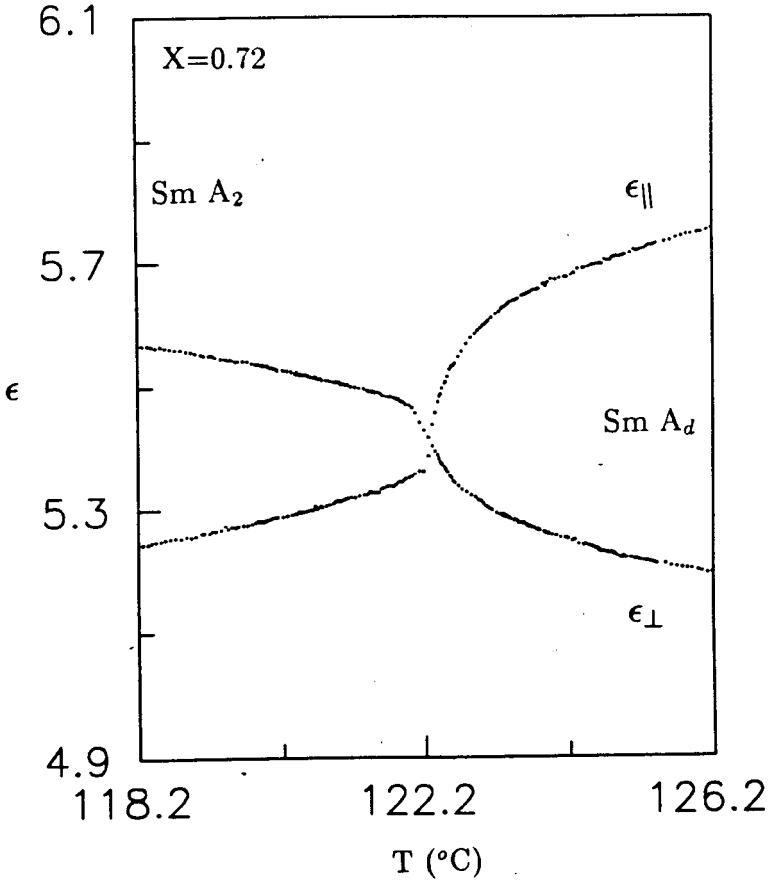

Figure 4.15: Thermal variation of $\epsilon_{\|}$ and $\epsilon_{\perp}$ for X=0.72.

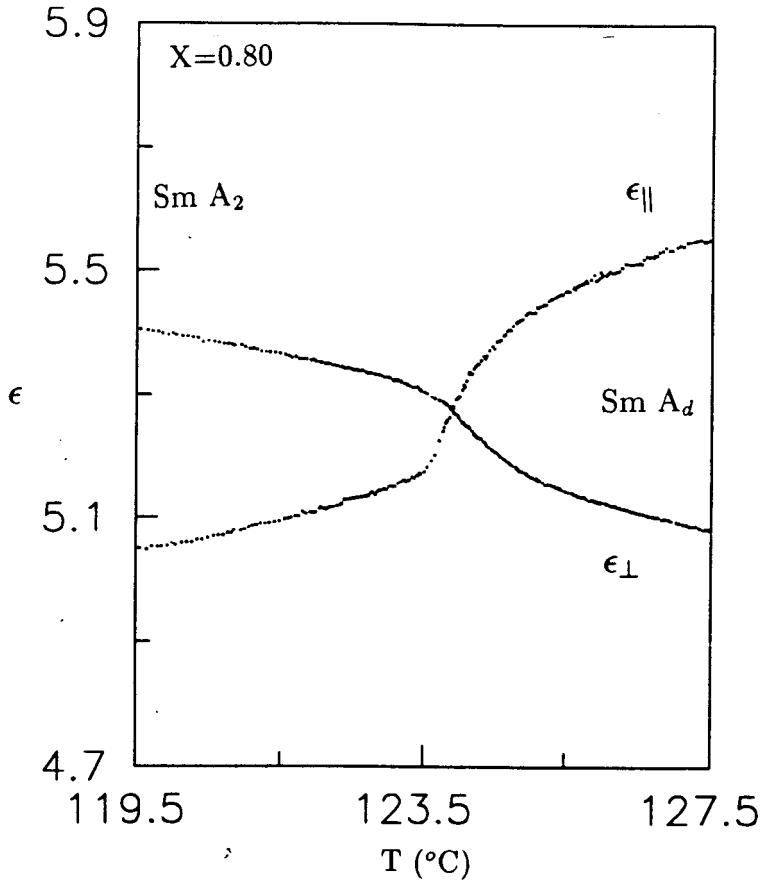

Figure 16: Thermal variation of $\epsilon_{\|}$ and $\epsilon_{\perp}$ for X=0.80.

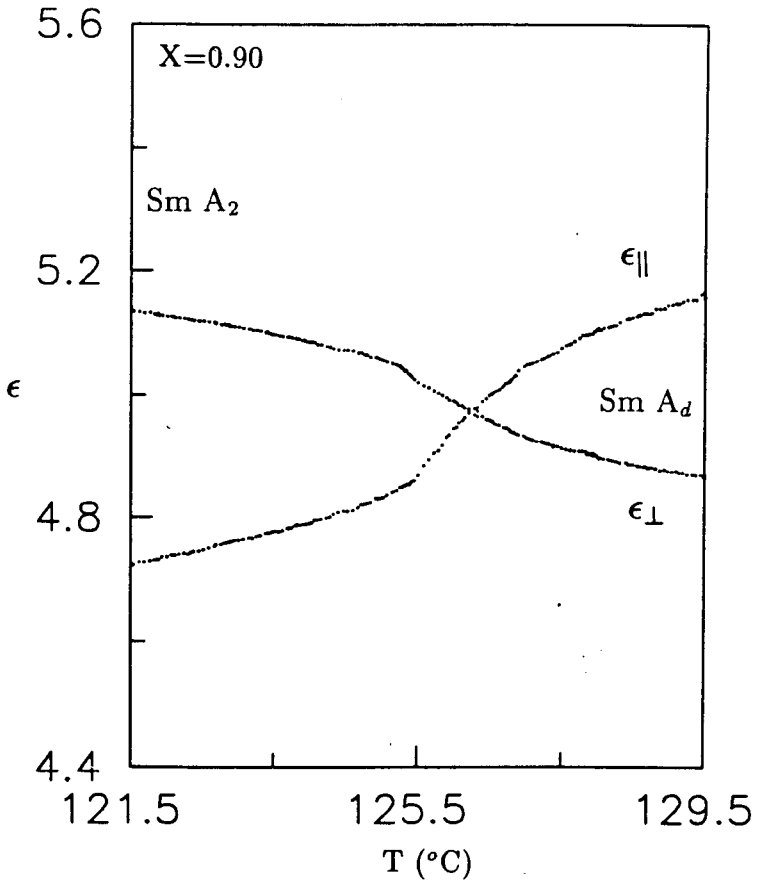

Figure 17: Thermal variation of $\epsilon_{\|}$ and $\epsilon_{\perp}$ for X=0.90.

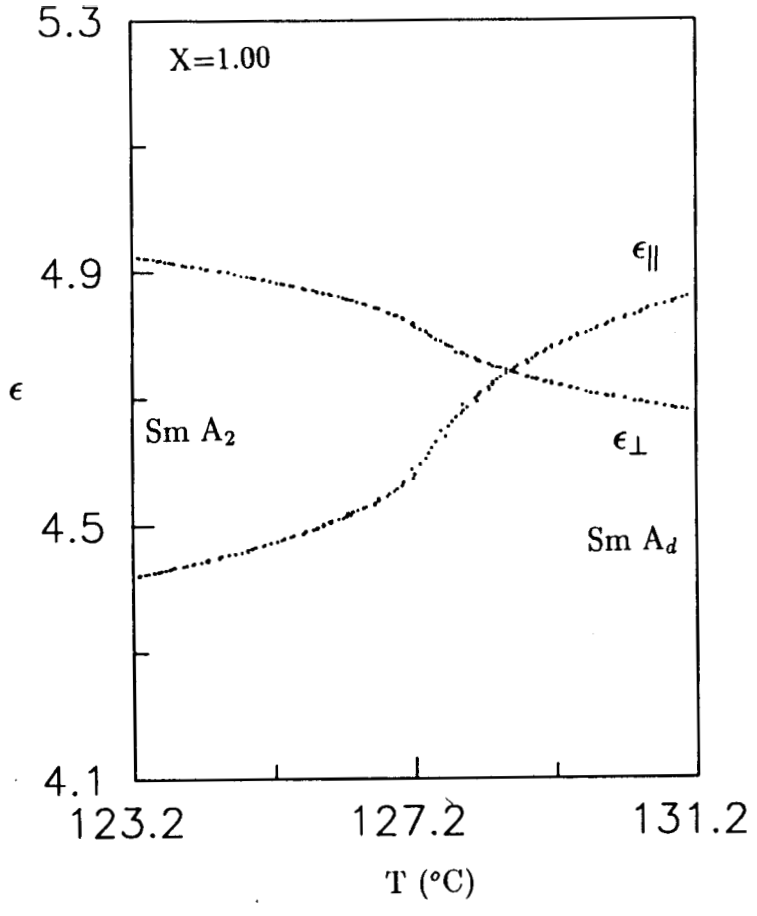

Figure 4.18: Thermal variation of $\epsilon_{\|}$ and $\epsilon_{\perp}$ for X=1.00 or 11OPCBOB.

0.72, 0.80, 0.9 and for pure 11OPCBOB respectively. For concentrations below $X \leq 0.65$, both $\epsilon_{\|}$ and $\epsilon_{\perp}$ show a steep variation across the transition, whereas for higher concentrations this variation is much smoother. As mentioned earlier X-ray studies[9] identified $X=0.642$ as the critical point concentration. Thus there is a first order transition for $X<0.642$ and a continuous evolution type without a phase transition for $X>0.642$. The change in the nature of the transformation manifests as a change in the steepness of the thermal variation of both $\epsilon_{\|}$ and $\epsilon_{\perp}$. Another point to be noted here is that there is a cross-over in the values of $\epsilon_{\|}$ and $\epsilon_{\perp}$ near the transition. Plots of dielectric anisotropy $(\Delta\epsilon = \epsilon_{\|} - \epsilon_{\perp})$ versus temperature for different concentrations are shown in figures 4.19-4.27. Although the steepness of the $\Delta\epsilon$ variation near the transition shows a concentration dependence, it was not significant enough to locate the critical point accurately.

In order to locate the critical point we proceeded as follows. The data of $\Delta\epsilon$ versus temperature was fitted to an expression of the form

$$\Delta\epsilon = A^{\pm}t^{B} + C(T - T_c) + D \qquad (4.12)$$

where $t = \frac{T - T_c}{T_c}$ is the reduced temperature and $C(T - T_c)$ represents the background contribution to $\Delta\epsilon$. D is the value of $\Delta\epsilon$ at T_c. A non-linear least square fit with all the parameters floating, was performed using the Marquardt algorithm.

It may be noted that a theoretical one-loop model[8] predicts a similar expression for the variation of specific heat. Equation 4.12 describes the data very well for all the mixtures studied. Figure 4.28 shows representative plots of the data for $X=0.55$, 0.63 & 0.72 along with the fit to equation 4.12. For comparison,

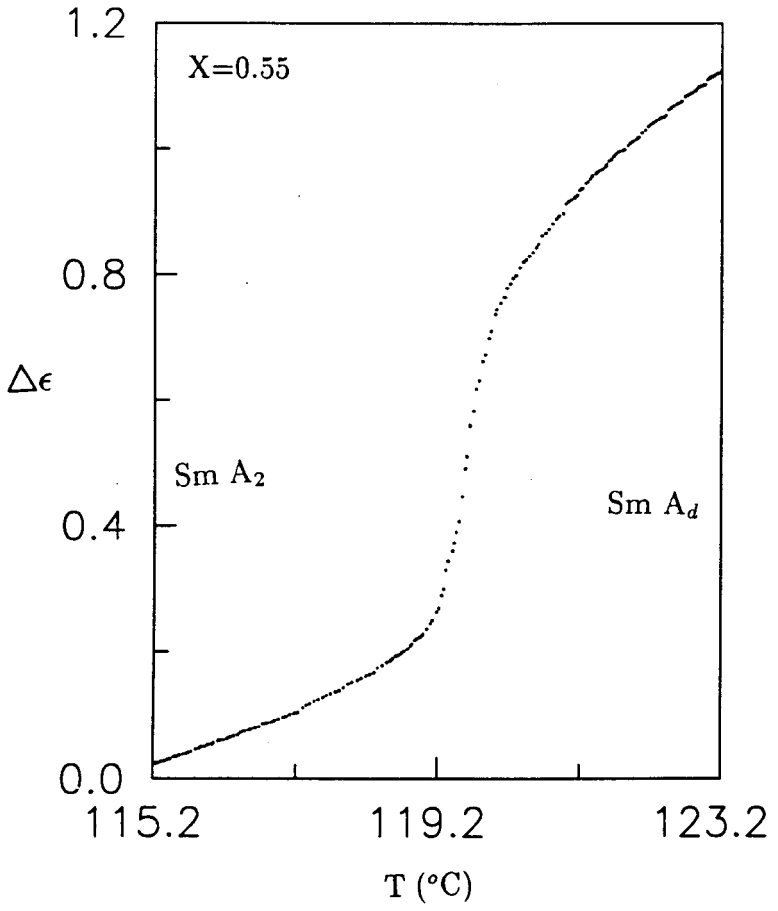

Figure 19: Thermal variation of dielectric anisotropy $\Delta\epsilon(=\epsilon_{\|}-\epsilon_{\perp})$ for X=0.55.

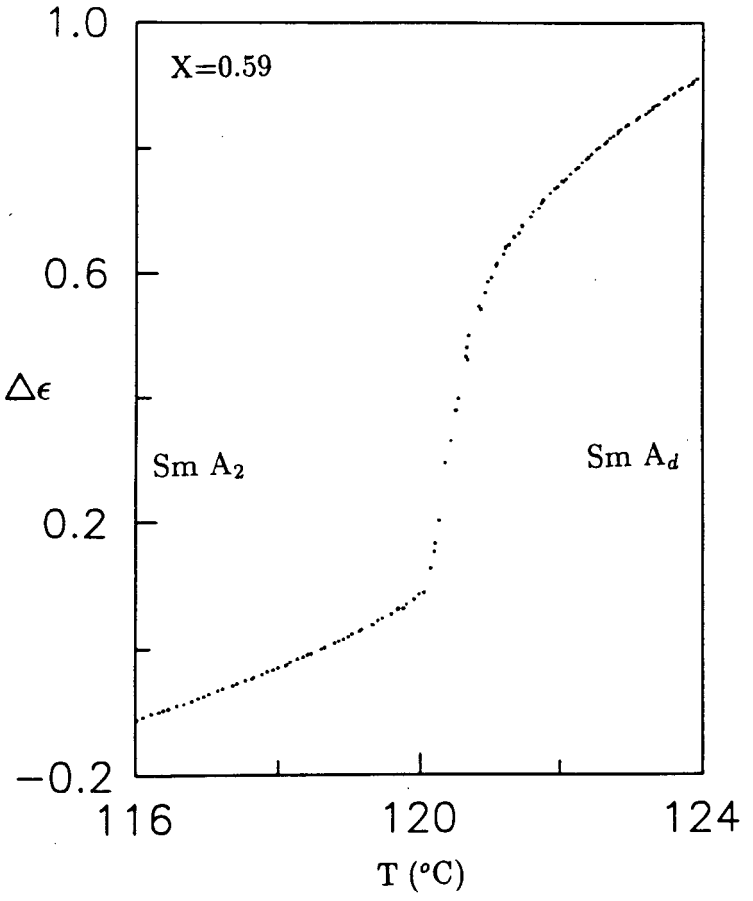

Figure 20: Thermal variation of $\Delta\epsilon$ for X=0.59.

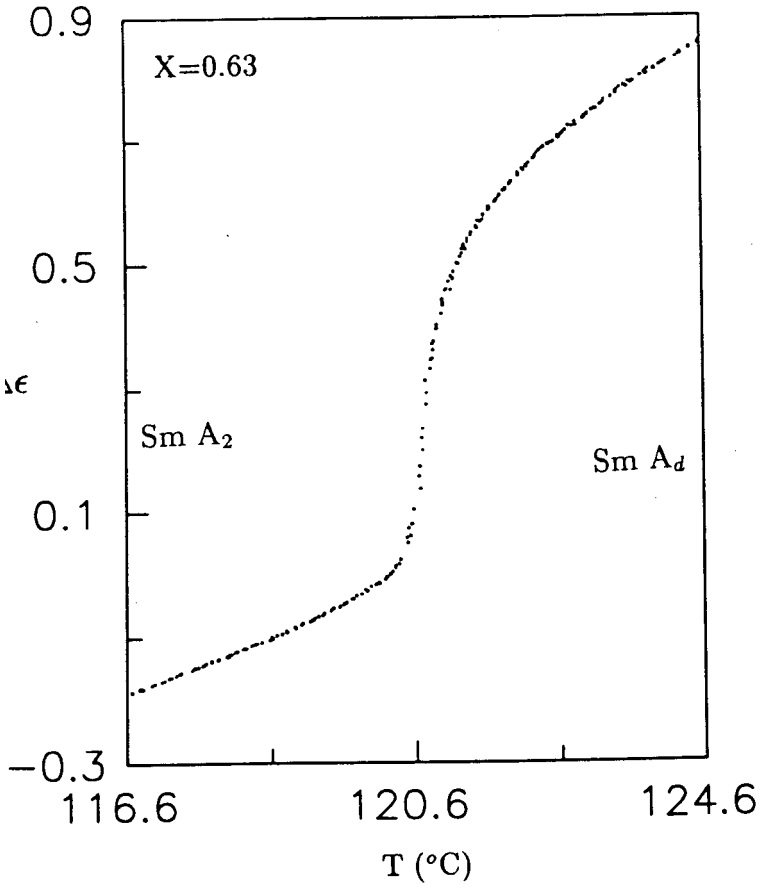

Figure 21: Temperature variation of $\Delta\epsilon$ for X=0.63.

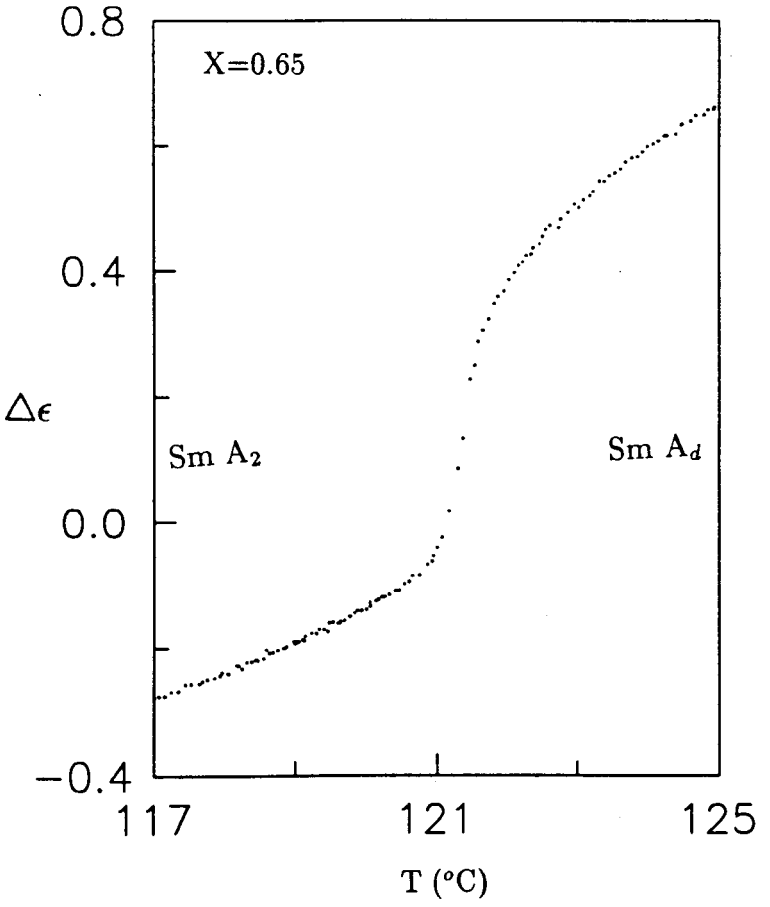

Figure 22: Temperature variation of $\Delta\epsilon$ for X=0.65.

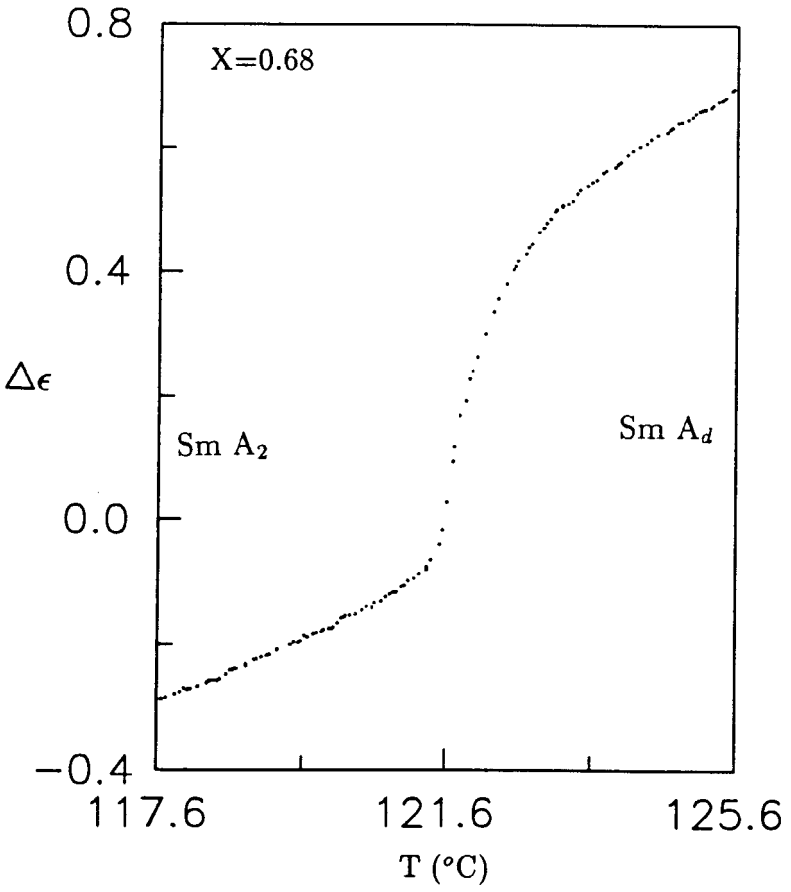

Figure 23: Thermal variation of $\Delta\epsilon$ for X=0.68.

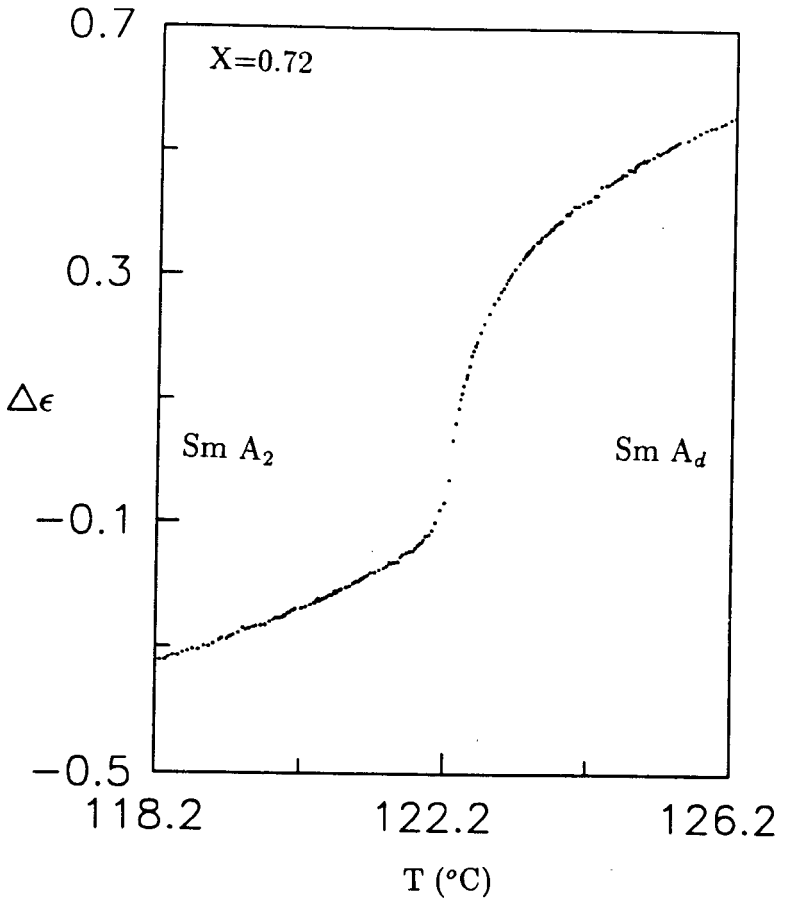

Figure 24: Thermal variation of $\Delta\epsilon$ for X=0.72.

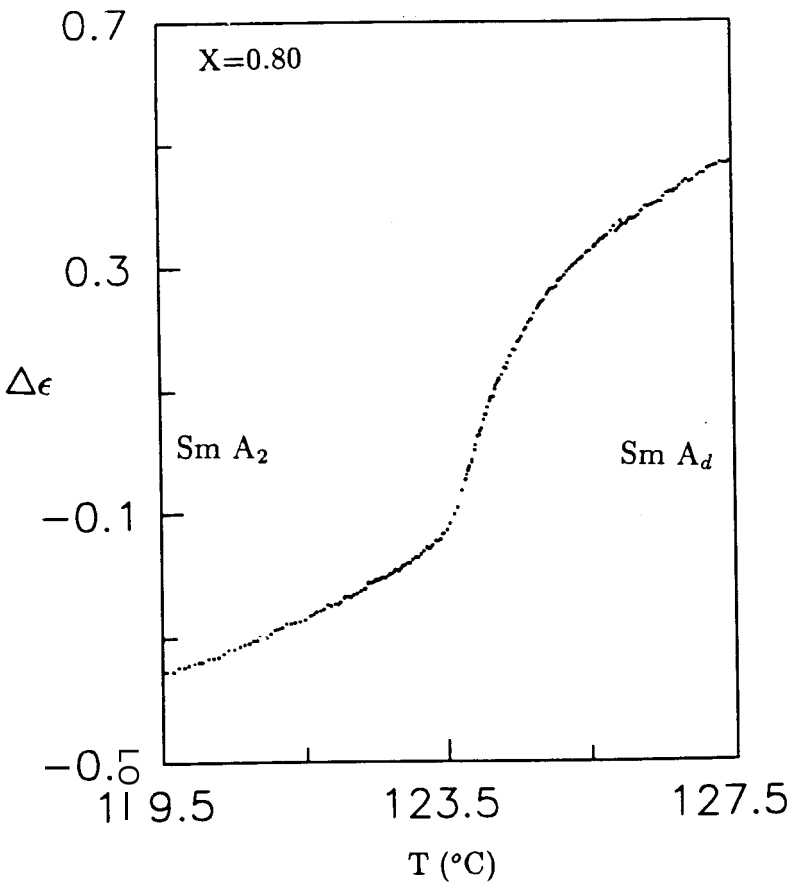

Figure 25: Thermal variation of $\Delta\epsilon$ for X=0.80.

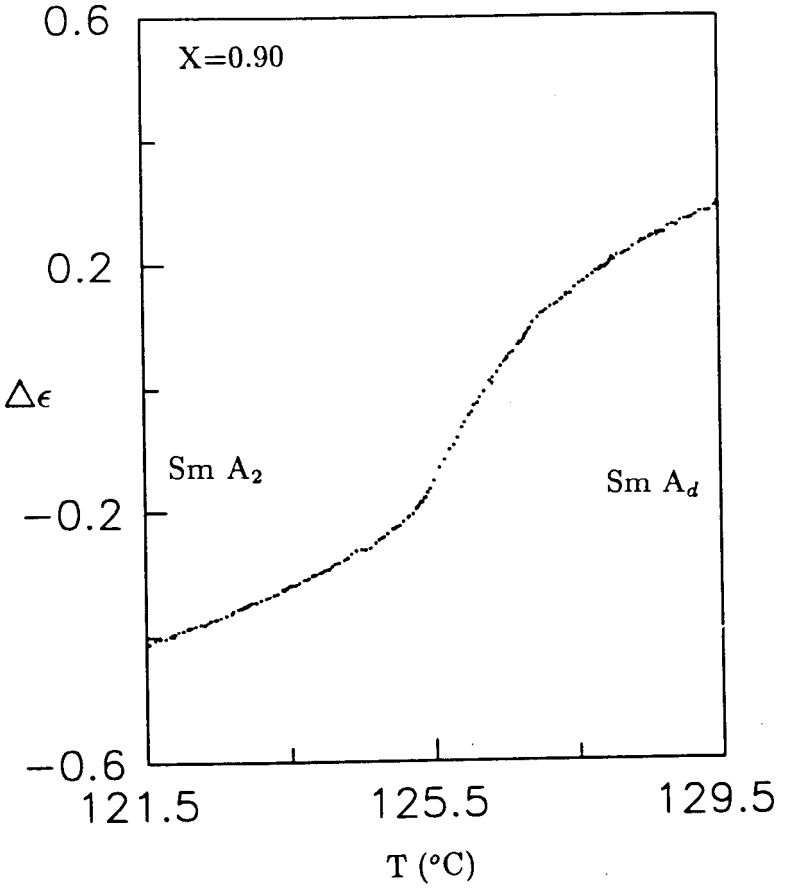

Figure 26: Thermal variation of $\Delta\epsilon$ for X=0.90.

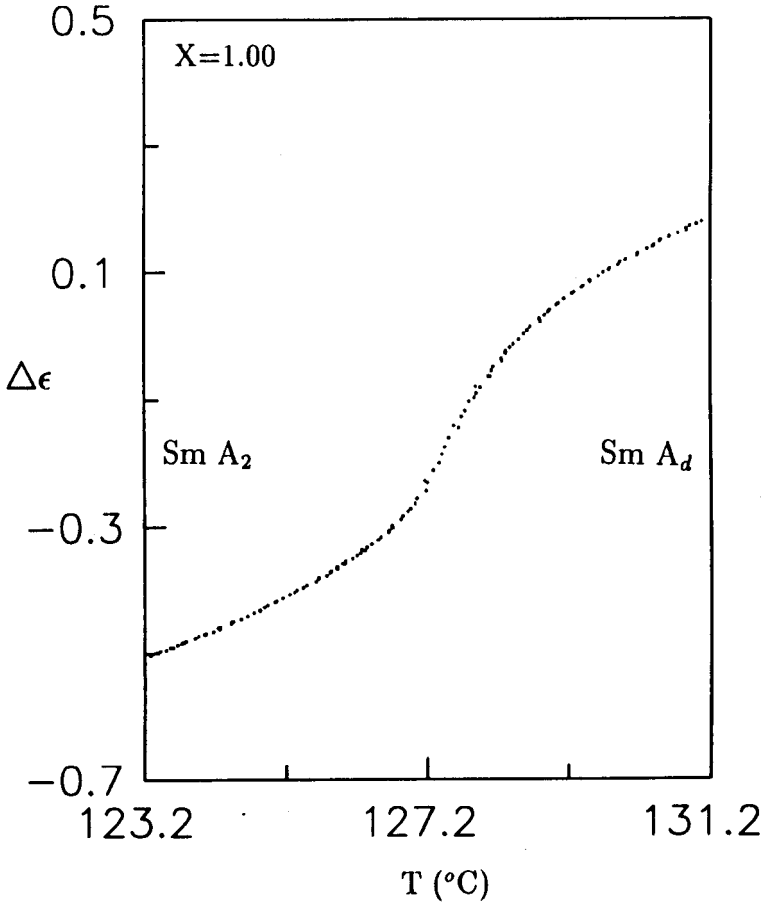

Figure 4.27: Thermal variation of $\Delta\epsilon$ for X=1.00, i.e., pure 11OPCBOB.

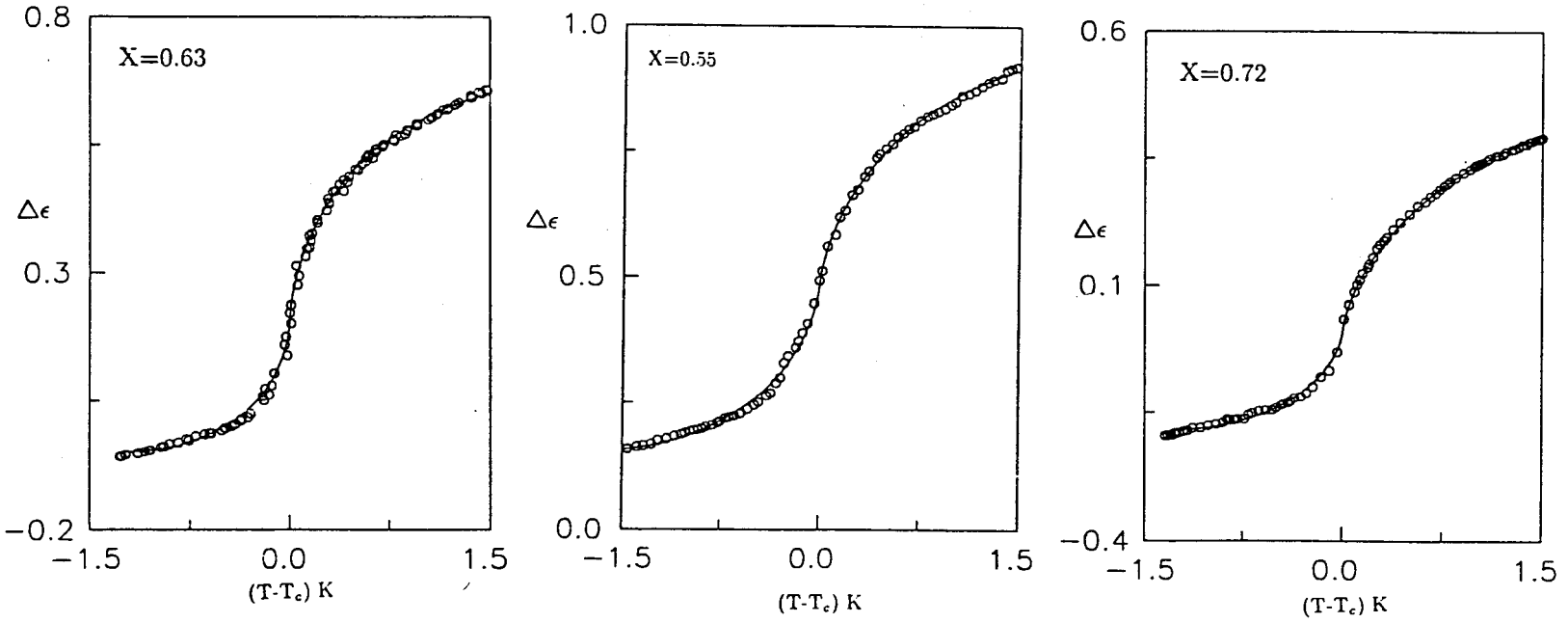

Figure 4.28: Representative plot showing fit to equation 4.12 for X=0.55, 0.63 and 0.72. Circles represent measured data points and solid line the fitting.

the X-ray data for X=0.642 for which a similar kind of fit was done by Jeong et al[10] is reproduced in the figure 4.29.

Figure 4.30 shows the thermal variation of $\frac{d}{dT}(\Delta\epsilon)$ calculated using the fit parameters $A^{\pm}$, B, C& D for different concentration. The salient features observed are as follows:

1. the peaks resemble very closely to the specific heat curves[10] obtained near the critical point.

2. The height of the peak is much larger and narrow for X=0.63 than for X<0.63 or X>0.63.

The peak heights obtained in this manner are plotted as a function of concentration in figure 4.31. It is seen that the peak height increases from either side (lower as well as higher concentrations) and reaches a maximum for X=0.64. We identify this concentration for which peak height attains a maximum as the *critical* point concentration. The critical point concentration X_c=0.64, obtained in this way, is in excellent agreement with the value obtained from both X-ray[g] and calorimetric[10] measurements.

4.2.3 Dispersion Studies

Dispersion measurements (parallel to the director) were carried out on X=0.63, (a concentration with a first order Sm A_d-Sm A_2 transition) to see whether there is a jump in the relaxation frequency f_R at the transition.

The measurements of frequency dependent dielectric constant ($\epsilon(\omega)$, with

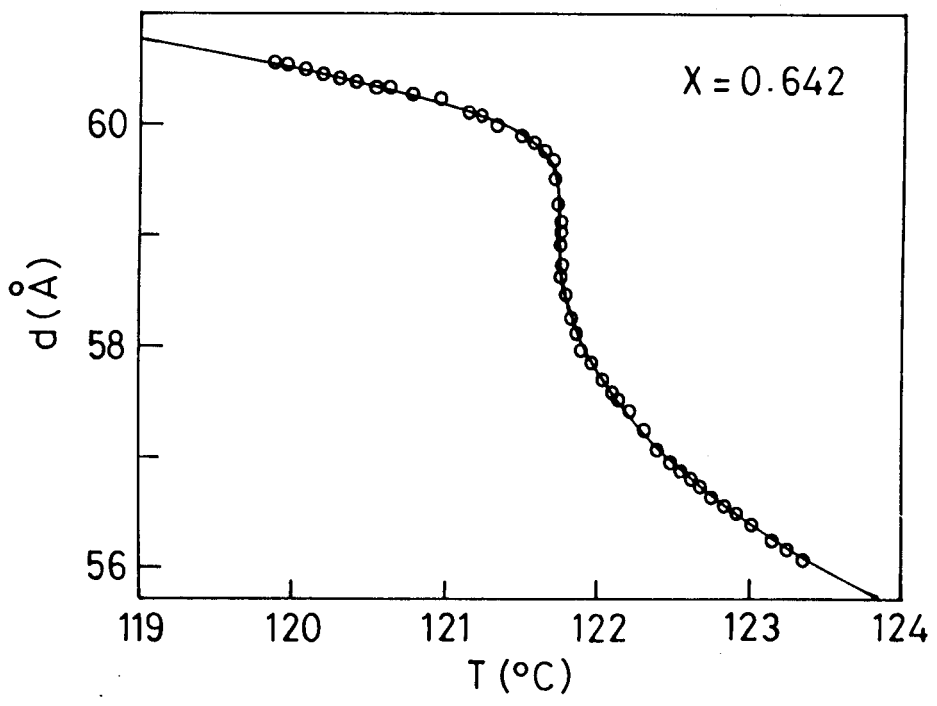

Figure 4.29: Fitting of the smectic layer spacing d to an expression similar to equation 4.12. (From Jeong et al[10]).

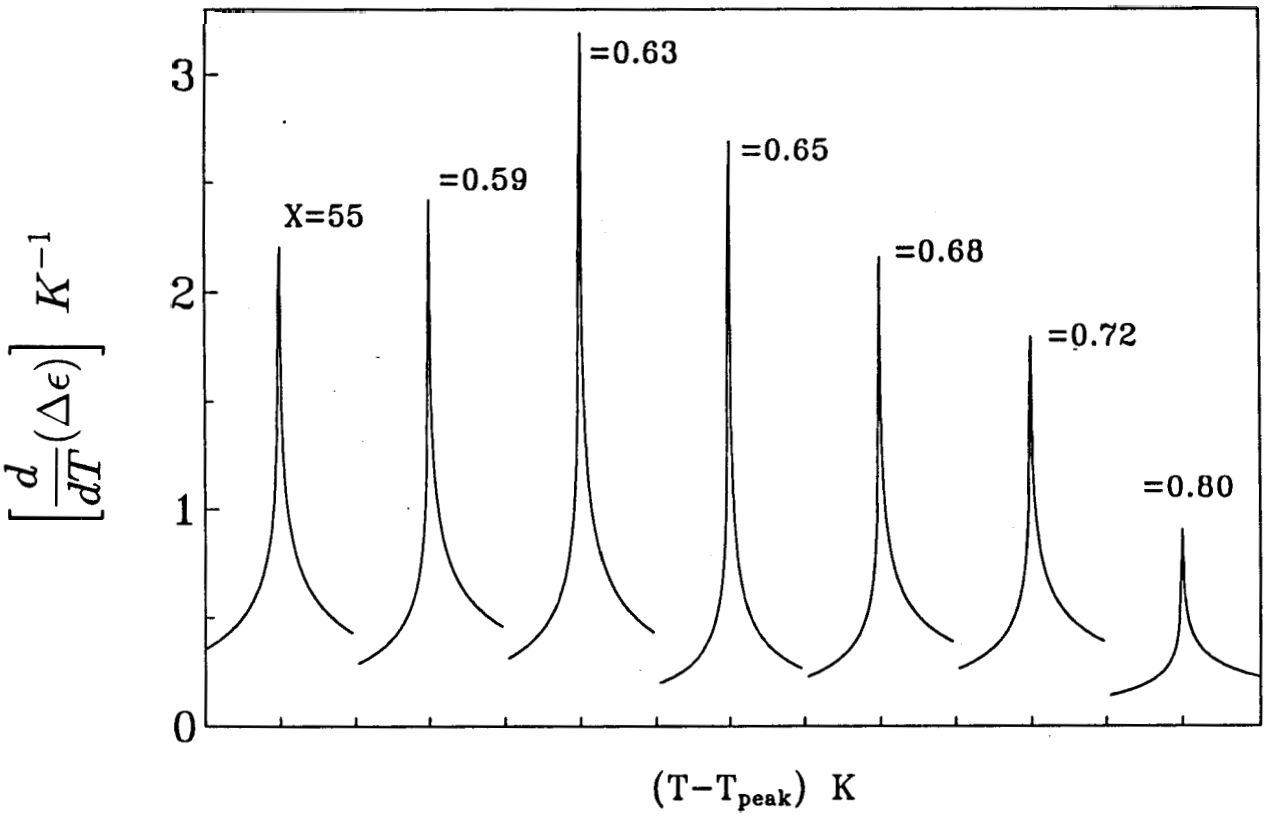

Figure **4.30:** Plot of $\frac{d}{dT}(\Delta\epsilon)$ as a function of reduced temperature T-T_{peak} for different concentrations. For the sake of presentation, the data lying within 0.5^{o}C of T_{peak} is shown.

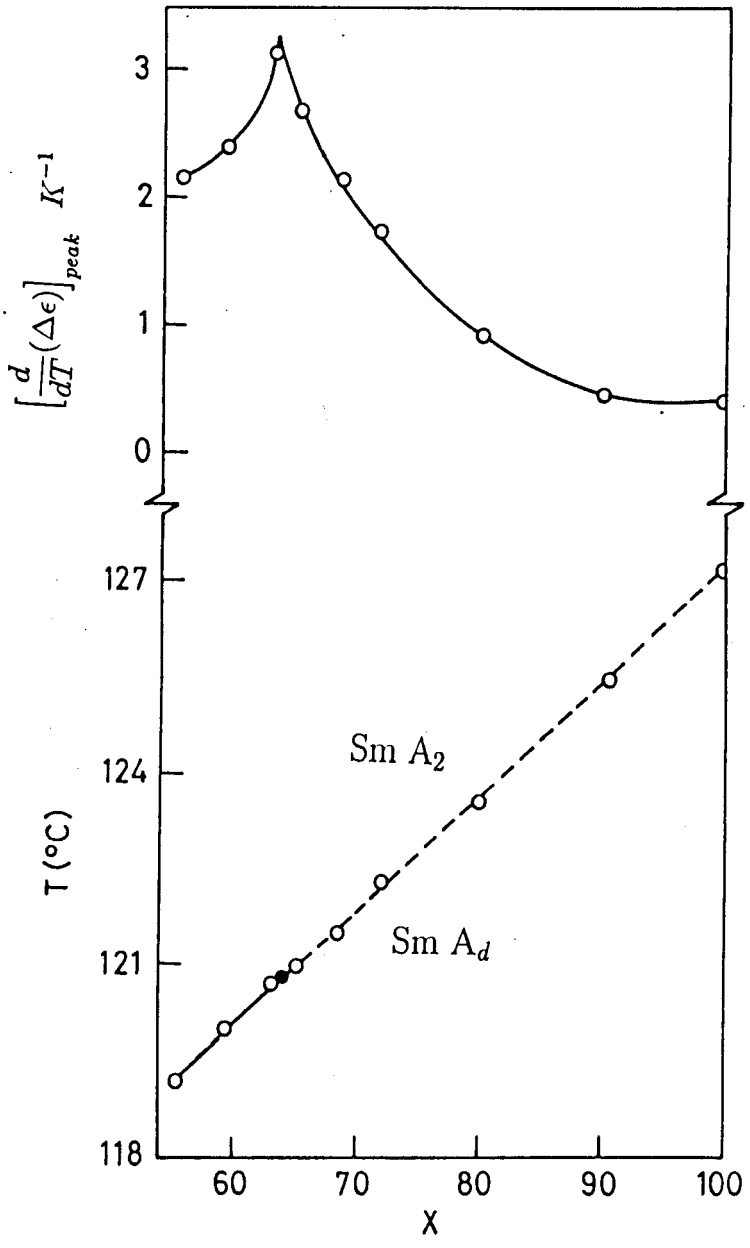

Figure 4.31: Top panel: Peak height of $\frac{d}{dT}(\Delta\epsilon)$ vs. T-T_{peak} curves, plotted as a function of X. Notice that $\left[\frac{d}{dT}(\Delta\epsilon)\right]_{peak}$ increases on moving from both X<0.64 and X>0.64 and reaches a maximum for X=0.64. Bottom panel: Partial T-X phase diagram of the binary system 11OPCBOB and 9OBCB. Solid line denote the Sm A_d-Sm A_2 transition boundary while the dashed line represent the locus of "inflection point" in the supercritical region. • → denotes the critical point estimated from peak height plots of $\frac{d}{dT}(\Delta\epsilon)$ curves.

$w = 2\pi \times frequency)$ were done by recording the capacitance and dissipation factor D while sweeping the frequency from 1kHz to 10MHz at a desired step value. Care was taken to collect more data in the neighbourhood of the relaxation frequency. During this dispersion scan the temperature was maintained constant to within ±10mK. The real part of the dielectric constant ϵ' is given by the ratio of capacitance of the sample to that of an empty cell, while the imaginary part ϵ'' is the product of ϵ' and D. The frequency dependence of the complex dielectric constant $\epsilon^*(\omega)$ is given by[16]

$$\epsilon^*(\omega) = \epsilon' - j\epsilon'' = \epsilon_\infty + \frac{\Delta\epsilon}{(1 + j\omega\tau)^{1-h}} \tag{4.13}$$

where $\Delta\epsilon(= \epsilon_0 - \epsilon_\infty)$ is the dielectric strength, ϵ_0 & ϵ_∞ are the values of dielectric constant at frequencies far below and far above f_R respectively, $\tau[= 1/(2\pi f_R)]$ the relaxation time, and h is a constant called the distribution parameter with $0 \leq h < 1$. When $h=0$ equation **4.13** reduces to a pure Debye type of relaxation.

Rationalising equation **4.13**

$$\epsilon' = \epsilon_\infty + \frac{Ar\left[1 + (\omega\tau)^{1-h}\sin(\pi h/2)\right]}{1 + (\omega\tau)^{2(1-h)} + 2(\omega\tau)^{1-h}\sin(\pi h/2)} \tag{4.14}$$

$$\epsilon'' = \frac{\Delta\epsilon(\omega\tau)^{1-h}\cos(\pi h/2)}{1 + (\omega\tau)^{2(1-h)} + 2(\omega\tau)^{1-h}\sin(\pi h/2)} \tag{4.15}$$

Real (ϵ') and imaginary (ϵ'') parts of the dielectric constant has been fitted to equation **4.14** & **4.15** respectively to obtain the dielectric strength $\Delta\epsilon$, the relaxation frequency f_R, ϵ_∞ and h. The fitting has been carried out using a non-linear least-square program based on the Marquardt algorithm by floating all the parameters involved.

Expressions 4.14 & 4.15 describe the data very well over the entire range of measurement. Further the distribution parameter h came out to be quite small ($\sim$ 0.05) indicating that the relaxation process is a pure Debye type. Representative loss curve (semi-log plot of ϵ'' versus frequency) and Cole-cole plots (plot of ϵ' & ϵ'') at $T_c = -5.86°C$, i.e., in the Sm A_2 phase are shown in figure 4.32. Also shown are the fitting obtained for the expression 4.14 & 4.15. Similar type of plots in the Sm A_d phase (T_c+5.9°C) and at a temperature close to T_c (T_c-0.1°C) are shown in figures 4.33 & 4.34.

Figure 4.35 shows a plot of f_R obtained in this way versus $1/T$ for X=0.63. The results show that there is a slight increase in the f_R value on passing from Sm A_d to the Sm A_2 phase. The activation energy, W for the relaxation process can be evaluated using the expression

$$f_R \propto e^{-W/kT} \tag{4.16}$$

where k is the Boltzmann constant. The values W calculated from the linear portion of the f_R versus $1/T$ plot in the Sm A_d and Sm A_2 phases are $W_{Sm\ A_d}$=0.39eV & $W_{Sm\ A_2}$=0.46eV. This type of difference has been observed earlier also on a different material showing a Sm A_d-Sm A_2 transition.[12,14] The fact that $W_{Sm\ A_2} > W_{Sm\ A_d}$ has been suggested to be indicative of a better packing of molecules in bilayer Sm A_2 phase.

4.2.4 Nature of the Sm A_d-Sm A_2 critical point

The theory of Barois et al.,[7] mentioned in section 4.1.1 is a mean field one. More recently, Park et al.,[8] developed a nonlinear elastic model to describe the Sm A_d-

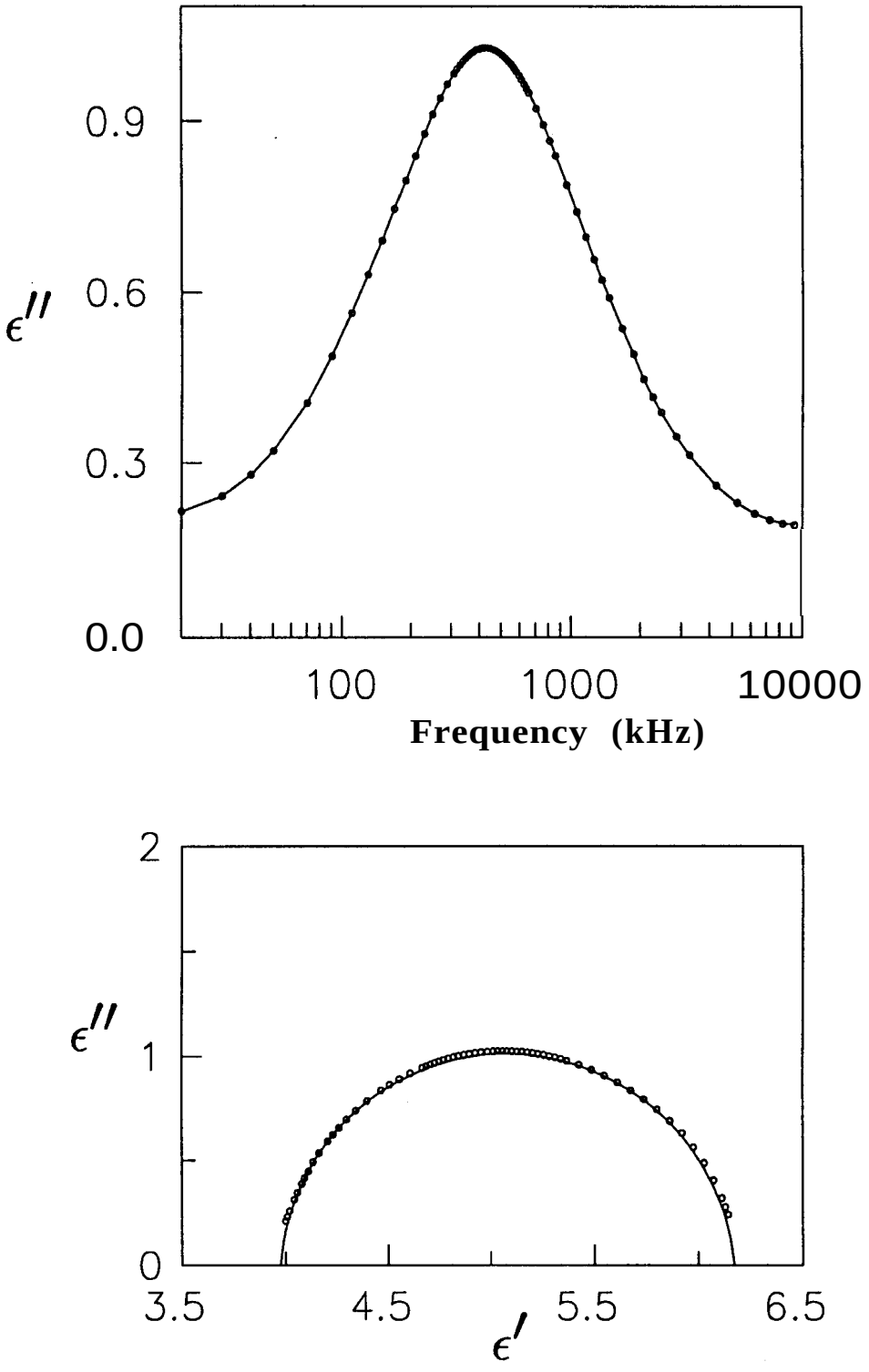

Figure 4.32: Top panel: Plot of ϵ'' vs. frequency(dielectric loss curve). Solid line is a fitting to equation 4.14. Bottom panel: Plot of ϵ'' vs. ϵ' plot (Cole-Cole plot) in the Sm A_2 phase($T-T_c = -5.86^oC$). Solid line is a fitting to equation 4.15.

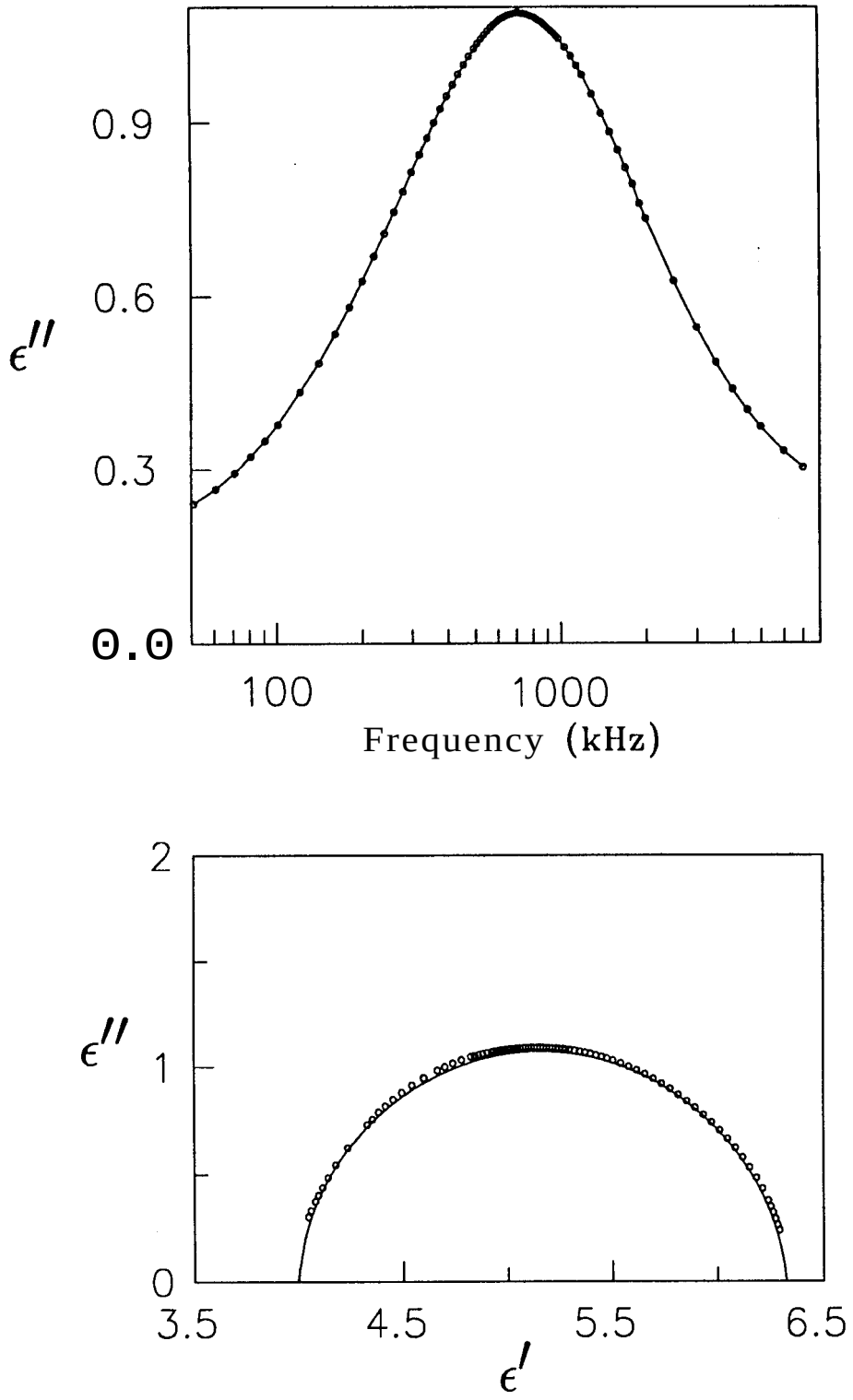

Figure 4.33: Top panel: Dielectric loss curve in the Sm A_2 phase ($T-T_c = -0.1°C$) near the Sm A_d-Sm A_2 transition. Solid line is a fitting to equation 4.14. Bottom panel: Corresponding Cole-Cole plot in the Sm A_2 phase. Solid line is a fitting to equation 4.15.

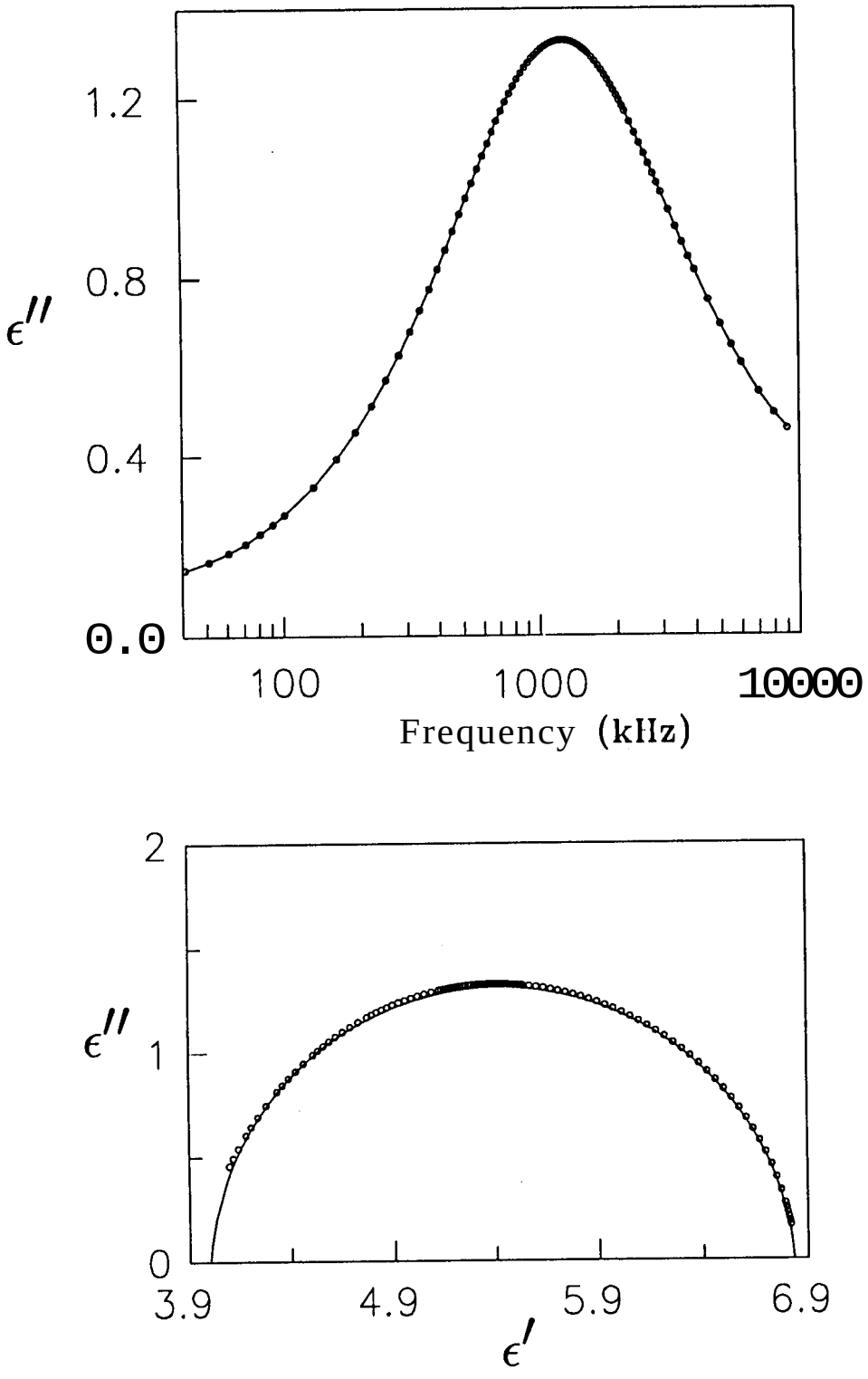

Figure 4.34: Top panel: Dielectric loss curve in the Sm A_d phase. ($T-T_c = +5.93°C$). Solid line is a fitting to equation 4.14. Bottom panel: Corresponding Cole-Cole plot in the Sm A_d phase. Solid line is a fitting to equation 4.15.

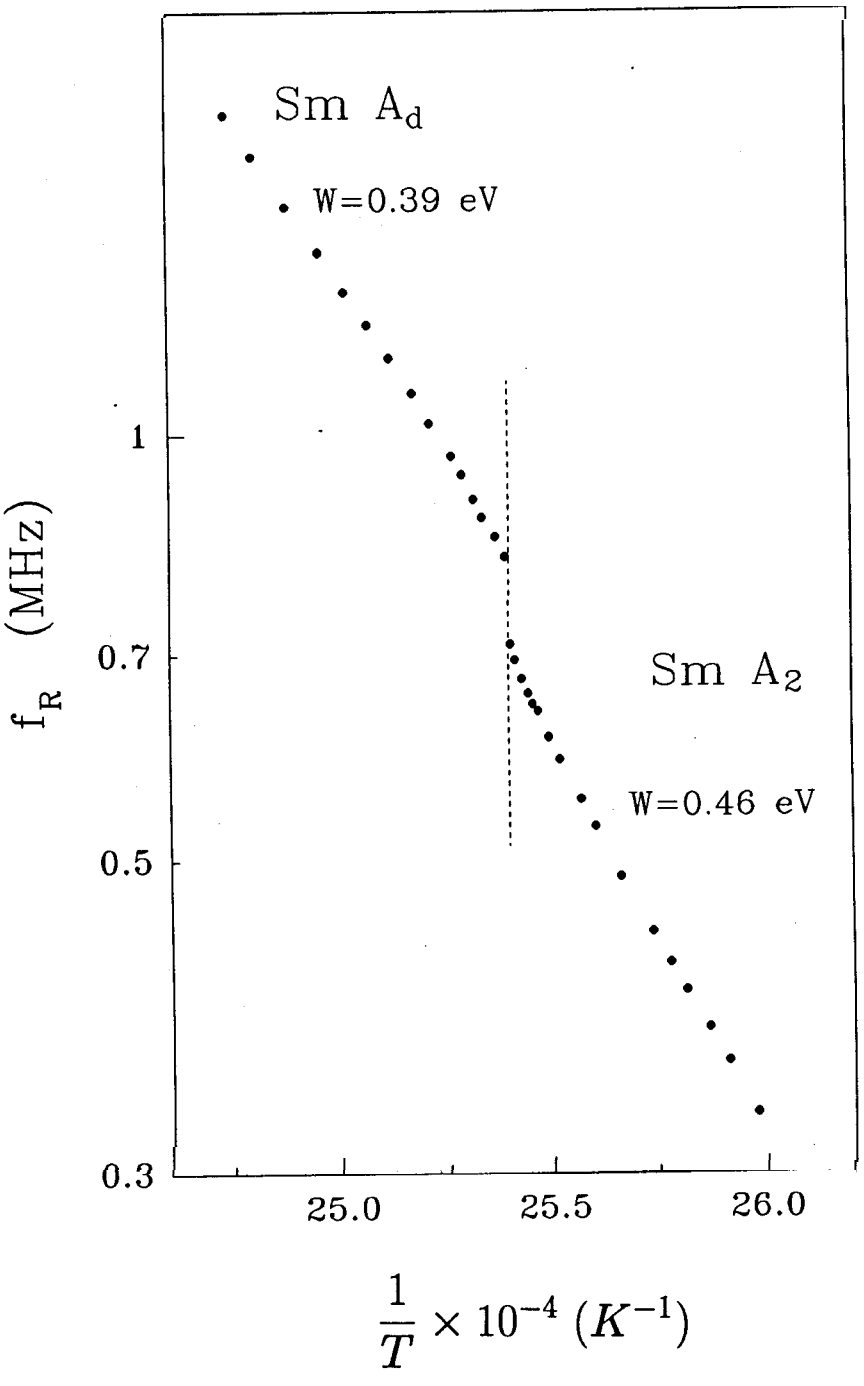

Figure 4.35: f_R **vs.** $1/T$ **plot for** X=0.63.

Sm A_2 critical point by taking into account fluctuations in the layer thickness. This theory predicts that the Sm A_d-Sm A_2 critical point should belong to a new universality class with d_u, the upper critical dimension, being six. (The upper critical dimension is defined as that dimension above which the system should exhibit mean field behaviour). The theory also predicts that the layer compressional elastic constant B vanishes at the critical point in exact analogy with the divergence of the bulk compressibility at the liquid-gas critical point. The specific heat at constant pressure and B along the critical pressure line should yield the exponent ν/Δ. On the other hand specific heat at constant layer spacing is expected to yield the exponent α. However, it has also been shown[17] that the upper critical dimension of the Sm A_d-Sm A_2 critical point drops to 2.5 when the splay-type critical fluctuations are suppressed by either a magnetic field or a local strain field. Heat capacity measurement across Sm A_d-Sm A_2 critical point (in the same binary system as in our study i.e., 11OPCBOB and 9OBCB) by Jeong et al.,[10] attempted to verify these theoretical predictions. The variation of specific heat in two near-critical mixtures with X=0.641 and 0.655 (X is the mole fraction of 11OPCBOB) are characterized by the critical exponent $\nu/\Delta = 0.6 \pm 0.2$. Smectic layer thickness for X=0.642 varied with an exponent $\nu/\Delta = 0.62$. The compressional-elastic-modulus(B) for X=0.67 (in the same binary system) varied with an exponent $\nu/\Delta = 0.4 \pm 0.01$.[18] Wen et al.,[19] did calorimetric measurements across Sm A_d-Sm A_2 critical point in mixtures of 11OPCBOB and its lower homologue 10OPCBOB. The variation of the heat capacity for three near-critical mixtures could be described by a simple power law with a critical exponent $\nu/\Delta = 0.45 \pm 0.08$. These experimental exponent

values, which are different from 3D-Ising model $\left(\nu/\Delta = 0.79\right)$ or the mean-field approximation $\left(\nu/\Delta = 0.67\right)$, support the theoretical prediction that the Sm A_d-Sm A_2 critical point belongs to a new universality class.

4.3 Continuous thermodynamic path between three smectic A phases of the same symmetry

The phase transition between the three polymorphic forms of smectic A phases, namely, Sm A_1, Sm A_d, Sm A_2, differing from each other only by the wavelength of their periodic modulations, are of considerable interest since all of them have the same macroscopic symmetry. As discussed in the previous sections of this chapter, there can only be a first order phase transition ,between Sm A_d and Sm A_2 as well as between Sm A_d and Sm A_1. Also it is seen both theoretically[7,8] and experimentally[9–10,19–20] that first order Sm A_d-Sm A_2 phase boundary terminates at a critical point beyond which Sm A_d phase evolves continuously into Sm A_2.

In the case of Sm A_d-Srn A_1 transition, two different situations have been dealt with theoretically.[21] In the mean field limit, the theory predicts the existence of a Sm A_d-Sm A_1 critical point similar to the Sm A_d-Sm A_2 critical point. However,,when the effect of fluctuations is considered the theory predicts that the Sm A_d-Sm A_1 boundary can end either as a critical point or in a nematic island. The theory also predicts several interesting results for the nematic island (see figure 4.36). The existence of two distinct critical endpoints (the points at which a second order line meets two first order boundaries) *a* & 6 on the

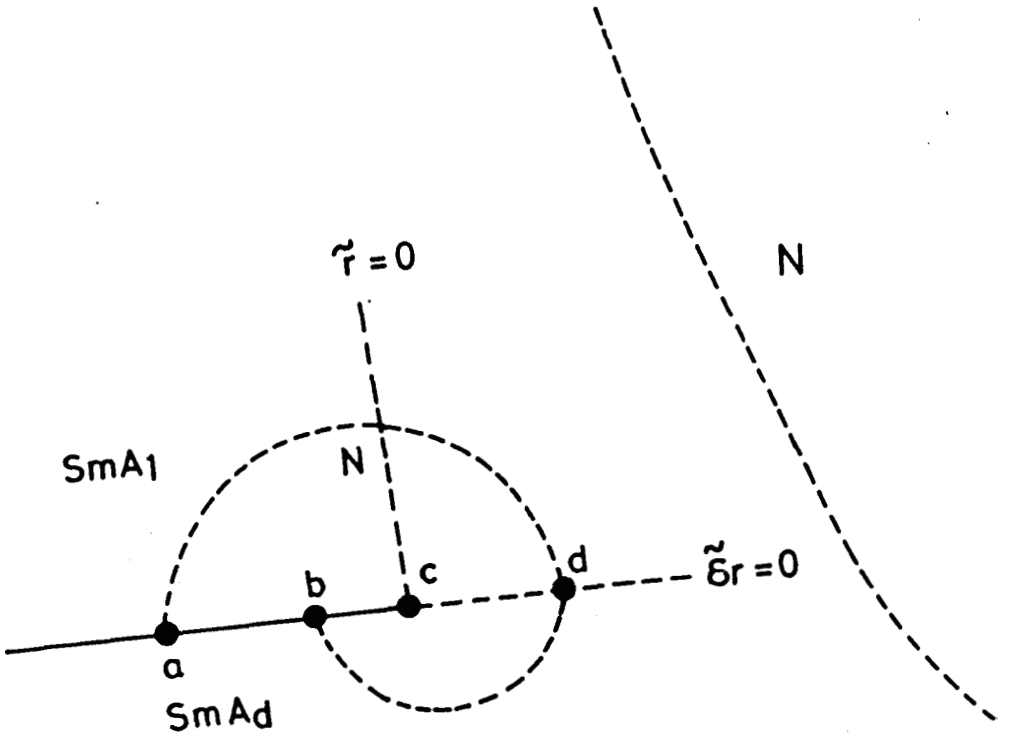

Figure 4.36: Theoretical phase diagram predicted by the dislocation-loop theory of Prost and Toner,[21] showing the nematic island at the terminus of the Sm A_d-Sm A_1 phase boundary. There are two types of nematics in this island, viz., N_d and N_1. c is the critical point at which a first order N_d-N_1 transition ends. *a* & b. are critical end points for the N_1-Sm A_1 and N_d-Sm A_d boundaries respectively. This nematic island is seen separated from the main domain nematic region. (From Ref.21).

continuous smectic A-nematic line which bounds the island, the first order line *(bc)* which separates two different types of nematic phases, N_d and N_1, and the termination of N_d-N_1 boundary at the critical point c (Figure 4.36). Prost and Toner[21] have also worked out a variety of possible phase diagrams that are consistent with the theory. Experimentally,[22–24] the closed-loop nematic domain at the termination of the first-order Sm A_d-Sm A_1 boundary as well as continuous evolutions between Sm A_d and Sm A_1 have been observed.

The Sm A_1-Sm A_2 transition, which was the first observed smectic A-smectic A transition[3] can either be second order or first order. The former is due to the exact doubling of the layer periodicity at the transition.

To our knowledge, both theoretically calculated[5–8] as well as experimentally observed[3,25] phase diagrams have always involved phase transitions (either first order or second order) on going from Sm A_1 to Sm A_2. However, the theoretical phase diagram (see figure **4.37)** proposed by Park et al.,[8] showed the possibility of a continuous path between Sm A_1 and Sm A_2 via Sm A_d phase. Experimentally such a continuous path has not been observed. The remaining part of this chapter discusses a novel result which shows the observation of continuous thermodynamic path between Sm A_1 and Sm A_2 phases. X-ray and optical studies show that this path, observed in a temperature-concentration diagram of binary liquid-crystal system, follows a continuous evolution from Sm A_1 to Sm A_2 via the Sm A_d phase.

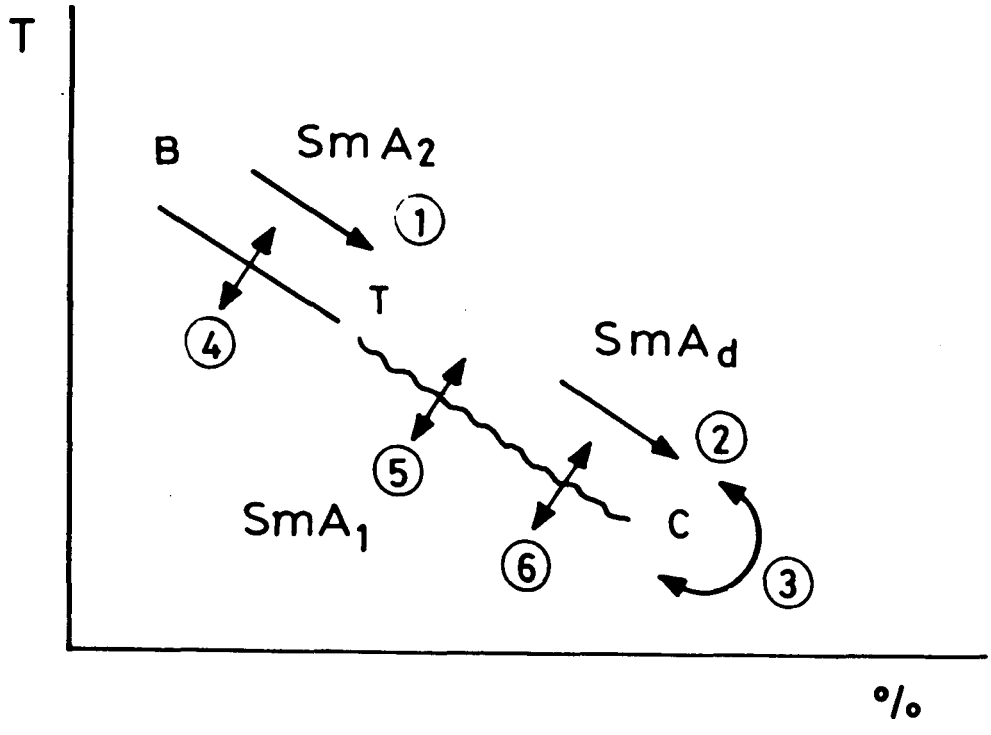

Figure 4.37: Possible phase diagram with different smectic A phases showing- a second order Sm A_1-Sm A_2 line(BT), a tricritical point(T) and a first order Sm A_1-Sm A_d line(TC) terminating in a critical point C. The paths indicated by the numbered arrows correspond to (1) continuous passage from Sm A2 to Sm Ad, (2) continuous passage between two Sm A_d phases of different layerspacings, **(3)** continuous passage from Sm A_d to Sm A_1, **(4)** a second order Sm A_1 to Sm A_2 transition and (5) & *(6)* first order Sm A_1 to Sm A_d transitions. (3) also shows possibility of a continuous path between Sm A_2 to Sm A_1 phases. (From Ref.8).

Studies on Sm A-Sm A phase boundaries

4.3.1 Experimental

Compounds used

The compounds used are 4-n-decyloxy-(4'-isothiocyanatopheny1)- benzoate or 10. O. NCS[26] and 11OPCBOB. The compound 10.O.NCS shows the Srn A_1 phase while 11OPCBOB shows, as mentioned already, a continuous evolution from Sm A_d to Sm A_2.[27] The structural formula and transition temperature: of 10.O.NCS are given in Table 4.2.

X-ray studies

Experiments were carried out on aligned samples obtained by cooling slowly from the nematic phase. For probing the transition between smectic A phases, two types of X-ray investigations were carried out. For the Sm A_d-Sm A_1 transition which involves large change in the layer spacing, d, a photographic setup was used. (These experiments were carried out at the Technical University of Berlin). In this case, the resolution in the determination of layer spacing d is $\pm 0.2\mathring{A}$, the temperature accuracy being $\pm$ 25 mK. For studying the Sm A_d-Sm A_2 transition where the change in d is small, the computer controlled guinier diffractometer described in Chapter 2 was used. In this case, precision in the determination of wave vector is $2\times10^{-4}\mathring{A}^{-1}$ while the resolution in the equatorial direction is $1\times10^{-3}\mathring{A}^{-1}$. The temperature was maintained to an accuracy of $\pm$5 mK.

10.O. NCS

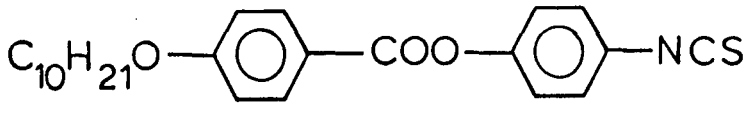

4–n–decyloxy - (4'-isothiocyanatophenyl) benzoate

Isotropic $\xrightarrow[96.0]{}$ Sm A

Table 4.2: Structural formula and transition temperature (in °C) of 10.O.NCS.

4.3.2 Results and Discussion

Mixing of 11OPCBOB in 10.O.NCS leads to a rich variety of phases and phase transitions between them. The temperature-concentration (T-X, X is the mole fraction of 11OPCBOB in the mixture) phase diagram of 10. O. NCS and 11OPCBOB is shown in figure 4.38. The phases were identified by optical microscopy in conjunction with X-ray studies on aligned samples. For all mixtures, Sm A_d phase is the higher-temperature smectic A phase, with Sm A_1 as the lower temperature phase for lower values of X and Sm A_2 for $0.8< X <1$. For intermediate X, the ribbon phase Sm $\tilde{C}$ is seen to intervene. For $0.48< X <0.67$ the Sm A_d and Sm A_1 phases are separated by a re-entrant nematic phase.

X-ray experiments have been carried out on four different concentrations, namely X=0.47, 0.69, 0.94 & 0.97. Figures 4.39-4.42 shows the thermal variation of layer spacing for all these concentrations. The results show that

1. For X=0.47, a continuous evolution between Sm A_d and Sm A_1 is seen (see figure 4.39).

2. First order Sm A_d-Sm A_1 transition marked by a jump in the layer spacing is seen for X=0.69 (see figure 4.40). The value of d drops from $50\mathring{A}$ to $32\mathring{A}$ at the transition.

3. Figure 4.41 shows a first order Sm A_d-Sm A_2 phase transition with a two phase coexistence region for X=0.94.

4. For X=0.97, Sm A_d is seen to evolve continuously to Sm A_2 phase without a phase transition (see figure 4.42).

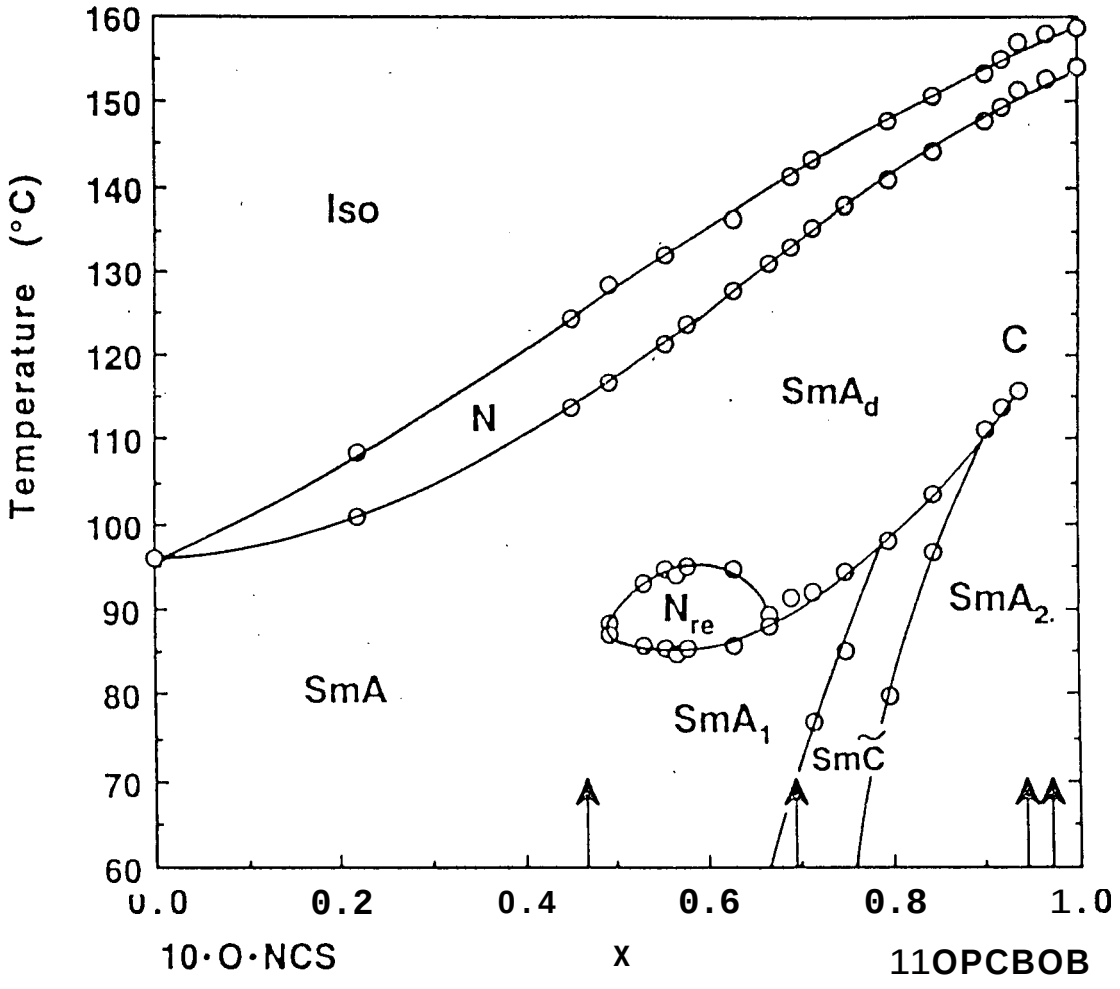

Figure 4.38: Temperature-concentraion (T-X) phase diagram of 10.O.NCS-11OPCBOB system. X is the mole fraction of 11OPCBOB in the mixture. The continuous evolution leading from Sm A_1 to Sm A_d surrounds the closed loop reentrant-nematic domain(N_{re}), while the supercritical evolution between Sm A_d and Sm A_2 is seen near the Sm A_d-Sm A_2 critical point C. Arrows indicate the concentrations of individual mixtures used for the X-ray experiments.

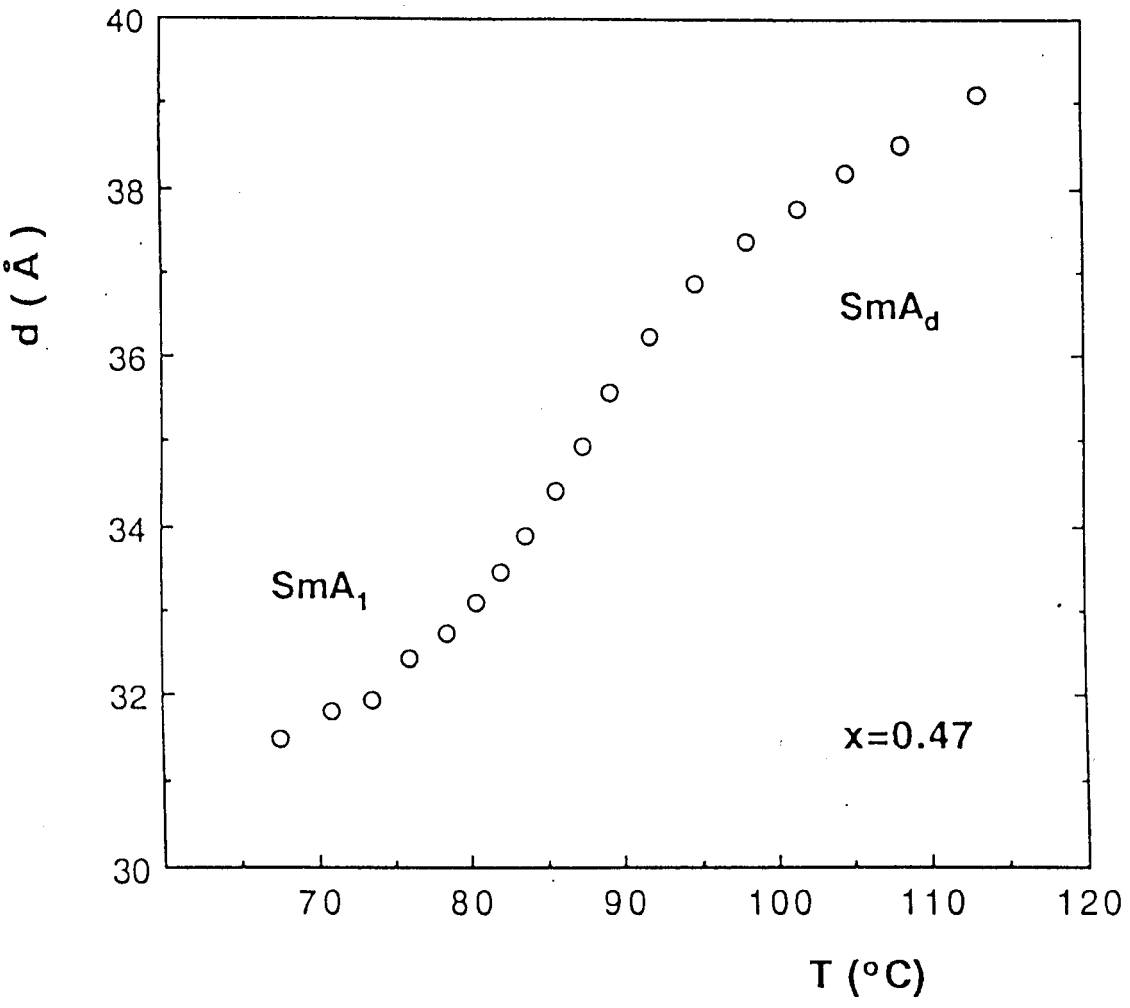

Figure 4.39: Temperature dependence of the smectic layer spacing d for X=0.47 showing a supercritical evolution from Sm A_d to Sm A_1 phase.

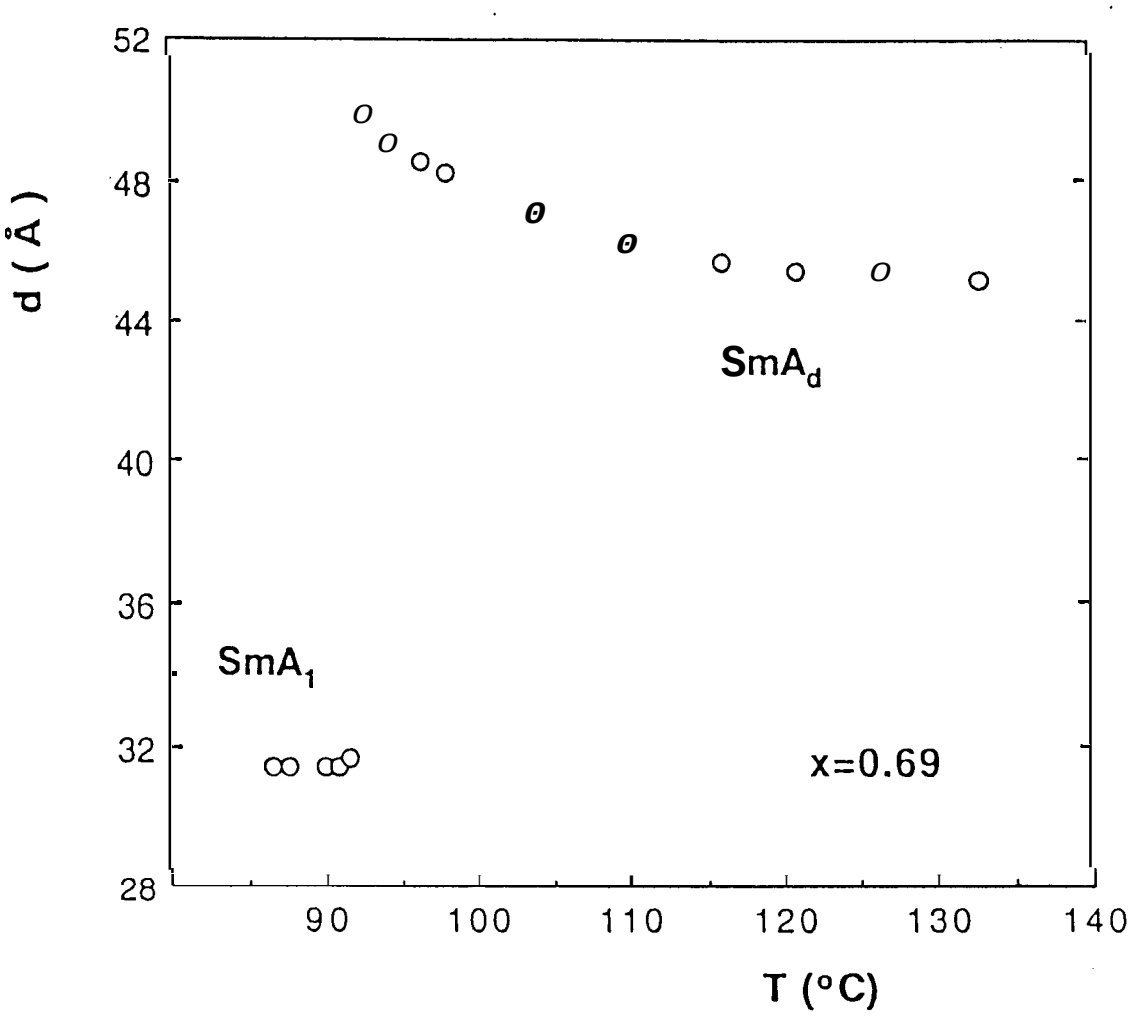

Figure 4.40: Thermal variation of d for X=0.69 exhibits a first order Sm A_d-Sm A_1 transition.

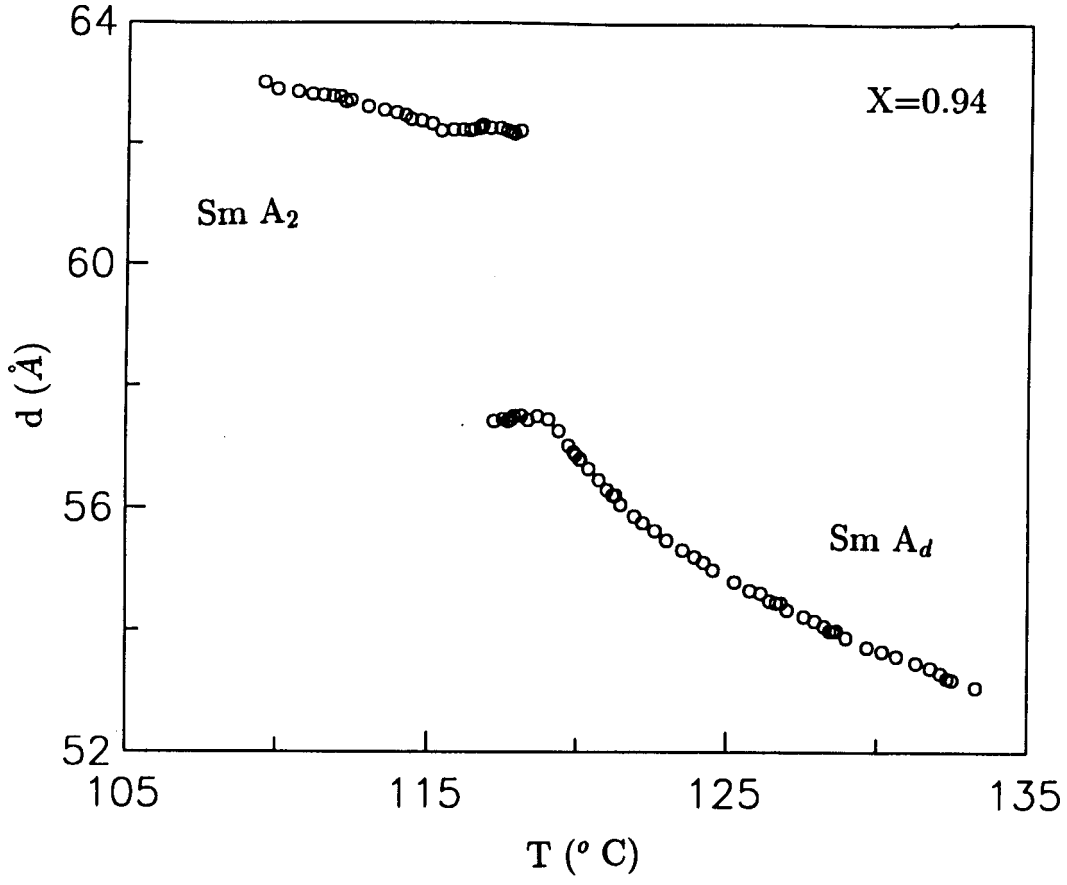

Figure 4.41: Temperature variation of d for X=0.94 shows a first order Sm A_d-Sm A_2 transition.

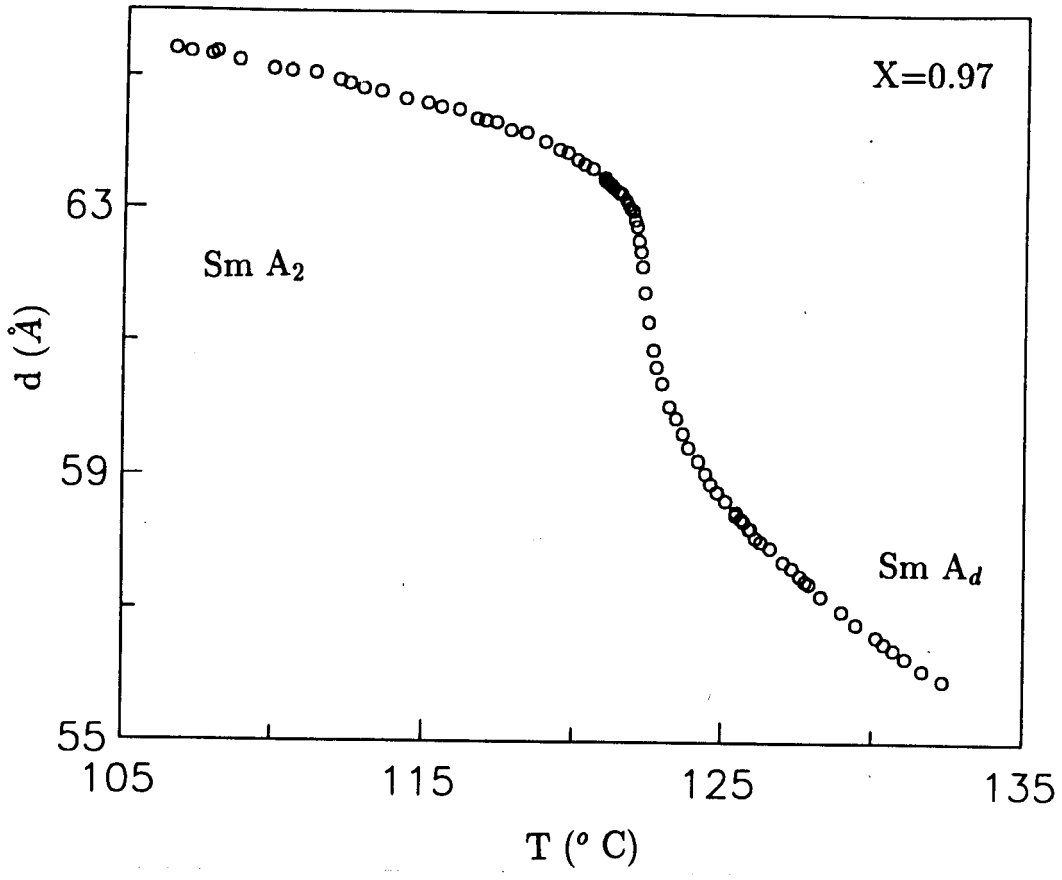

Figure 4.42: Temperature variation of d for X=0.97 shows a continuous evolution from Sm A_d to Sm A_2 phase.

Thus it is clear that the first order Sm A_d-Sm A_2 phase boundary is terminating at a critical point C, followed by a region of continuous evolution, with the critical point concentration lying between X=0.94 and X=0.97. Absence of Sm $\tilde{C}$ between Sm A_d and Sm A_2 for X>0.94 has been confirmed by careful optical studies. These studies, carried out by slowly cooling a homeotropically aligned sample across the transition, did not show any birefringence, characteristic of the onset of Sm $\tilde{C}$ phase. A similar experiment, carried out on X<0.90 mixtures, clearly showed a narrow region of the Sm $\tilde{C}$ phase.

Thus the phase diagram given in figure **4.38** shows that there exists a continuous thermodynamic path between Sm A_1 and Sm A_2 phases. This path is seen to traverse via a Sm A_d phase, i.e., Sm A_1 first evolves continuously into Sm A_d and then into Sm A_2, thereby showing that the global symmetry of Sm A_1, Sm A_d and Sm A_2 phases are the same.

Another interesting aspect of the phase diagram is that the Sm A_d-Sm A_2 part of the phase boundary terminates at a critical point, while the Sm A_d-Sm A_1 part of the boundary ends as a closed-loop nematic domain. Although the existence of Sm A_d-Sm A_2 critical point as well as a closed loop nematic domain at the terminus of Sm A_d-Sm A_1 has been predicted theoretically[7-8,21] and observed experimentally,[9-10,19-20,22-24] the possibility of their existing together at the two ends of the phase boundary in a single phase diagram has not been considered before. Our experimental phase diagram shows the occurrence of such a situation.

It should also be noted that the occurrence of Sm $\tilde{C}$ phase in the phase diagram is in accordance with the theoretical phase diagram. It is expected that Sm C is stable instead of Sm A in the vicinity of partially bilayer Sm A_d.[28]

References

[1] N.V.Madhusudana and S.Chandrasekhar, Proc. Int. Liq. Cryst. Conf. Bangalore, *Pramana Suppl.*, **1,** 57 (1973).

[2] A.J.Leadbetter, J.C.Frost, J.P.Gaughan, G.W.Gray and A.Mosley, *J.de.Phys.*, **40**, 375 (1979).

[3] G.Sigaud, F.Hardouin, M.F.Achard and H.Gasparoux, *J.Phys.(Paris) Colloq.* 40, C3-356 (1979); G.Sigaud, F.Hardouin and M.F.Achard, *Phys.Lett.*, **72A**, 24 (1979).

[4] F.Hardouin, A.M.Levelut, J.J.Benattar and G.Sigaud, *Solid State Commun.*, 33, 337 (1980).

[5] J.Prost, *J.de.Phys.*, **40**, 581 (1979).

[6] J.Prost and P.Barois, *J.Chim.Phys.*, 80, 65 (1983); J.Prost, *Liquid Crystals of one and two dimensional order,* edited by W.Helfrich and G.Heppke (Springer-Verlag, Berlin, 1980), p125.

[7] P.Barois, J.Prost and T.C.Lubensky, *J.de.Phys.*, 46, 391 (1985).

[8] Y.Park, T.C.Lubensky, P.Barois and J.Prost, *Phys.Rev.* A 37, 2197 (1988).

[9] R.Shashidhar, B.R.Ratna, S.Krishna Prasad, S.Somasekhar and G.Heppke, *Phys.Rev.Lett., 59,* 1209 (1987).

[10] Y.H.Jeong, G.Nounesis, C.W.Garland and R.Shashidhar, *Phys.Rev.* A 40, 4022 (1989).

[11] N.R.Njeumo, J.P.Parneix, C.Legrand, N.H.Tinh and C.Destrade, *J.de.Phys.*, 47, 903 (1986).

[12] C.N.Nagabushan, Experimental studies on the dielectric properties of liquid crystals Ph.D. Thesis, University of Mysore, 1988.

[13] S.Pfieffer, Polar liquid crystals: Dielectric, X-ray and miscibility investigations on smectic phases Ph.D. Thesis, Technical University Berlin, 1989.

[14] B.R.Ratna, C.Nagabushan, V.N.Raja, R.Shashidhar and S.Chandrasekhar, *Mol.Cryst.*Liq.Cyst., 136, 245 (1986).

[15] 11OPCBOB and 9OBCB are kindly given to us by Prof. G.Heppke.

[16] See e.g., Dielectric properties and molecular behaviour, N.E.Hill, W.E.Vaubhan, A.H.Price and M.Davies, Edited by T.M.Sugden, Van Nostrand *Reinhold* Company Ltd., London.

[17] Y.Park, T.C.Lubensky and J.Prost, *Liq.Cryst.*, 4, 435 (1989).

[18] J.Prost, J.Pommier, J.C.Rouillon, J.P.Marcerou, P.Barois, M.Benzekri, A.Babeau and H.T.Nguyen, *Phys.Rev.* B 42, 2521 (1990).

[19] X.Wen, C.W.Garland, R.Shashidhar and P.Barois, Phys.*Rev.* B 45, 5131 (1992).

[20] S.Quentel, G.Heppke, S.Krishna Prasad, S.Pfeiffer and R.Shashidhar, Mol.Cyst.Liq.*Cryst.*, 7, 85 (1990).

[21] J.Prost and J.Toner, *Phys.Rev.* **A** 36, 5008 (1987).

[22] P.E.Cladis and H.R.Brand, *Phys.*Rev.Lett., 52, 2261 (1984).

[23] F.Hardouin, M.F.Achard, Nguyen Huu Tinh and G.Sigaud, Mol.*Cryst.*Liq.*Cryst.*Lett., **3,** 7 (1986).

[24] R.Shashidhar and B.R.Ratna, *Liq.Cryst.,* 5, 421 (1989) and references therein.

[25] K.K.Chan, P.S.Pershan, L.B.Sorensen and F.Hardouin, *Phys.Rev.Lett.,* 54, 1694 (1985).

[26] G.Heppke, S.Pfeiffer, A.Ranft and R.Shashidhar, *Mol.Cryst.Liq.Cryst.,* 206, 31 (1991).

[27] S.Krishna Prasad, R.Shashidhar, B.R.Ratna, B.K.Sadashiva, G.Heppke and S.Pfeiffer, *Liq. Cyst.,* 2, 111 (1987).

[28] P.Barois, J.Pommier and J.Prost, *Solitons in Liquid Crystals,* edited by L.Lam and J.Prost(Springer-Verlag, Berlin), Chap 6.